Fermi National Accelerator Laboratory

FERMILAB-Pub-93/040-T
JHU-TIPAC-930008
MAD/PH/747
MSUHEP 93/05
NUB 3060-93 TH
NUHEP-TH-93-13
UCD-93-5
June 1993

The Strongly Interacting WW System: Gold–Plated Modes

J. Bagger,[a] V. Barger,[b] K. Cheung,[c] J. Gunion,[d] T. Han,[e]

G. A. Ladinsky,[f] R. Rosenfeld[g] and C.–P. Yuan[f]

(a) *Department of Physics and Astronomy, The Johns Hopkins University, Baltimore, MD 21218*

(b) *Department of Physics, University of Wisconsin, Madison, WI 53706*

(c) *Department of Physics, Northwestern University, Evanston, IL 60208*

(d) *Davis Institute for High Energy Physics, Department of Physics, University of California at Davis, Davis, CA 95616*

(e) *Fermi National Accelerator Laboratory, P.O. Box 500, Batavia, IL 60510*

(f) *Department of Physics and Astronomy, Michigan State University, East Lansing, MI 48824*

(g) *Department of Physics, Northeastern University, Boston, MA 02115*

ABSTRACT

In this paper we survey the signals and backgrounds for a strongly-interacting electroweak symmetry breaking sector at hadron supercolliders in the TeV region. We study the process $pp \to WWX$, and compute the rates for the "gold-plated" channels, where $W^{\pm} \to \ell^{\pm}\nu$ and $Z \to \ell^{+}\ell^{-}$ ($\ell = e, \mu$), for a wide variety of models. Using a forward jet-tag, a central jet-veto and a back-to-back lepton cut to suppress the Standard Model backgrounds, we demonstrate that the SSC and LHC have substantial sensitivity to strong interactions in the electroweak symmetry breaking sector.

Operated by Universities Research Association Inc. under contract with the United States Department of Energy

1. Introduction

During the past decade, the discovery of the W and the Z bosons demonstrated that the gauge structure of the Standard Model (SM) is correct. However, little is known about the mechanism that gives the vector bosons their mass. In the Standard Model, they acquire mass because a scalar field, the Higgs doublet, has a nonzero vacuum expectation value v. At present, however, there is no experimental evidence in favor of the Higgs particle: all the precision measurements can be described by a Higgs-free Standard Model.

Of course, the Standard Model without a Higgs boson cannot be a fundamental theory [1,2]. It is only an effective theory, breaking down below a few TeV. New physics must emerge below this scale – which the next round of accelerators had better be prepared to find!

WW scattering provides a particularly promising avenue for investigating this new physics (here and henceforth W generically denotes the W or Z boson, unless specified otherwise). The $WW \to WW$ cross section without a light Higgs boson violates perturbative unitarity at about 1 TeV. Consequently, new physics must couple to this channel in just such a way as to cure its bad high energy behavior.

In this paper we will investigate signals and backgrounds for the process $pp \to WWX$ at hadron supercolliders, such as the SSC and LHC. We will concentrate on the situation in which there are no new particles below a TeV. We shall study a variety of possible models, all of which are perfectly consistent with the data to date.

Of course, in such studies one must decide what is the "signal" and what is the "background." We will take the *signal* to be the process $pp \to W_L W_L X$, as shown in Fig. 1, where L refers to longitudinal polarization (while the transverse polarization will be denoted by T). This definition of the signal is appropriate because the $W_L W_L$ channels couple most strongly for new physics, and $W_L W_L$ production is negligible unless the interactions among the W's are strong. Since we are mainly interested in physics for the electroweak symmetry breaking sector, we will not include the contributions to our $W_L W_L$ signal from Yukawa couplings, such as $t\bar{t}H$ in the SM. The most difficult *background* to the $W_L W_L$ final state is $W_L W_T$ and $W_T W_T$ production: $pp \to W_L W_T X$ and $pp \to W_T W_T X$. Such processes are a background in the sense that their cross sections are essentially independent of strong interactions in the W sector, *i.e.* they are insensitive to new physics. Further, this background is irreducible in that the final state contains two real W's analogous to the signal of interest (ignoring polarization).

Ultimately, after appropriate cuts, the $W_L W_T + W_T W_T$ background is dominated by the "electroweak" (EW) diagrams, as shown in Fig. 2a, which includes $W_T W_T, W_L W_T$ scattering diagrams and those in which W's are radiated or emitted via electroweak interactions. An additional contribution to the $W_T W_L + W_T W_T$ background arises from the $q\bar{q}$ annihilation processes illustrated in Fig. 2b. Since both of these backgrounds are essentially independent

of the new physics in the W_LW_L channel, we are free to compute them using the Standard Model with a light (100 GeV) Higgs, for which W_LW_L production is negligible. The difference between this computation and a first-principles computation of the background in a model which incorporates strong interactions in the W_LW_L sector is negligible at the energies we consider. Finally, there are heavy quark backgrounds, especially those associated with top quark production and decay, Fig. 2c. These too may be reliably computed in the SM once the top-quark mass is known.

For most of our signal estimates, we will simplify our calculations by using the Goldstone-boson Equivalence Theorem [1-3], which states that, at high energies, the external longitudinal vector bosons can be replaced by their corresponding would-be Goldstone bosons. This is both a computational and conceptual simplification, for it allows us to draw on our considerable experience with Goldstone-boson scattering in QCD. We will also use the effective W approximation [4,5] to connect the W_LW_L subprocesses to the pp initial state.

We focus our attention on the "gold-plated" events, where the W and Z decay to charged leptonic final states ($\ell = e, \mu$). For the purpose of this study, we ignore final states where the bosons decay hadronically, as well as final states where either of the Z's decays into neutrinos. These final states should also be studied and will possibly improve the observability of electroweak symmetry breaking at the SSC/LHC [6].

Because we focus on the gold-plated leptonic channels, the only backgrounds to the W_LW_L signal that we need to consider are those in which real W_LW_T and W_TW_T pairs are produced. As already noted, in the final analysis, the diagrams in Fig. 2a yield the most difficult backgrounds. We suppress these backgrounds by imposing further restrictions on the events. However, we must also deal with the additional background processes of Figs. 2b and 2c. The continuum pair production processes of Fig. 2b arising from $q\bar{q}$ annihilation (which we term the QCD background) contribute to the W^+W^-, $W^\pm Z$ and ZZ channels. At lowest order, these annihilation processes have a very different final state structure than the WW scattering processes of interest, where spectator quark jets are left behind when the incoming quarks radiate the initial-state W's that then scatter (see Fig. 1). Thus, even allowing for higher-order radiation corrections, the QCD background can be greatly suppressed by requiring a tagged forward jet. The heavy top quark processes of Fig. 2c, arising from $t\bar{t}$, $t\bar{t}W$ and $t\bar{t}Z$ production followed by t and $\bar{t}$ decays to real W's, contribute to the W^+W^-, $W^\pm Z$ and $W^\pm W^\pm$ channels. Fortunately, these top quark background processes have substantial jet activity at moderate rapidity and can be efficiently suppressed by requiring a central jet-veto.

Indeed, it turns out that both the forward jet-tag and the central jet-veto are effective in reducing the backgrounds from the irreducible $LT + TT$ electroweak backgrounds as well. Nonetheless, if only jet-tagging and/or vetoing is applied, a substantial EW $LT + TT$ background remains in the $W^\pm W^\pm$ and W^+W^- channels. This background remnant can be greatly reduced with little impact on the LL signal by requiring energetic leptons at low

rapidity, and especially requiring that the two leptons appearing in the final state be very back-to-back.

Because we use the effective W approximation for our signal, we can only estimate the effects of the tag and veto cuts. We use the exact Standard Model calculation with a 1 TeV Higgs to derive efficiencies for these cuts. Since these efficiencies should be relatively model-independent, we can apply them to the effective W calculations to estimate the rate for each signal. The efficiency for the lepton cuts, including the back-to-back requirements if imposed, is obtained by employing the effective W approximation and decaying the final W's appropriately. The accuracy of this procedure was tested in the SM 1 TeV Higgs case. Good agreement was found between the lepton cut efficiencies obtained in the exact calculation and in the effective W calculation.

In section 2 of this paper we study these procedures for the Standard Model. We take the signal to be a 1 TeV Higgs resonance, and the electroweak background to be the SM rate for a light Higgs boson (we employ $m_H = 100$ GeV). We present the cuts that maximize the signal/background ratio while preserving a reasonable rate. We use the exact calculation to compute efficiencies for the forward jet-tag and the central jet-veto. In section 3 we present the different models we will employ. We examine resonant and nonresonant scenarios, and frame our discussion in the language of chiral lagrangians. In section 4 we examine the accuracy of our procedure in which we apply the cut efficiencies obtained from the exact SM calculation of section 2 to the cross sections obtained using the equivalence theorem and the effective W approximation. We then present our basic numerical results and assess the reach of the SSC and the LHC for each of the strongly interacting W-system models. Section 5 contains further discussion and comments. We conclude with some brief remarks in section 6.

2. Standard Model

In this section, we discuss WW scattering in the Standard Model with a 1 TeV Higgs particle. Although it is argued [7] that the SM is not a consistent effective theory if $m_H \gtrsim 800$ GeV or so, we take this case as a prototype for models with strong WW scattering. We present the signal and the background, calculated using the exact, order α^2, matrix elements for $pp \to WWX$. We use these results to derive efficiencies for the forward jet-tag and the central jet-veto. The comparison of signal results to those found using the equivalence theorem and the effective W approximation will be presented in sections 4 and 5.

In this study we concentrate on the purely leptonic decay modes of the final state W's, namely the "gold-plated" events, with $W^\pm \to \ell^\pm \nu_\ell$ and $Z \to \ell^+\ell^-$ ($\ell = e, \mu$). The experimental signature is given by two or more isolated, charged leptons in the central rapidity ($y(\ell)$) region, with large transverse momenta (p_T). Although clean, these gold-plated channels carry the price of relatively small branching fractions for the purely leptonic W decays.

The diagram for longitudinal vector boson scattering is given symbolically in Fig. 1,

$$qq \rightarrow qqW_LW_L \ , \tag{2.1}$$

where W_L denotes a longitudinally-polarized vector boson ($W_L = W_L^{\pm}$, Z_L). If the interactions between W_L bosons are strong at high energies, we expect W_LW_L scattering to be enhanced at large invariant mass. It is this enhancement which defines the signal we wish to isolate.

The irreducible backgrounds are shown in Fig. 2. At least one of the final W's produced in the background processes is transversely polarized. In particular, the cross sections for WW scattering to produce W_LW_T or W_TW_T pairs are essentially independent of the Higgs mass in the SM and are part of the background by definition. Other backgrounds include gluon-exchange between quarks with initial and final state emission of two W's (both of which are dominantly transversely polarized) [8], and a variety of electroweak processes in which a final W_T arises via bremsstrahlung or emission from a primary quark or electroweak boson line. Continuum WW pair production arising from $q\bar{q}$ annihilation and gg fusion also contributes to the background. For cases with a $W^{\pm}$ in the final state, there is an especially important *reducible* background from heavy quark production and decay.

It is important to note that two spectator quarks always emerge in association with the W_LW_L scattering signal, but that spectators emerge in only a subset of the irreducible backgrounds. The spectator quarks usually appear in forward/backward regions, and have an energy of order one TeV and a p_T of order $M_W/2$. It is therefore possible to improve the signal/background ratio by tagging those quark jets (in particular, continuum pair production processes do not have a spectator quark jet at lowest order in perturbation theory) [9]. While studies have shown that tagging *two* high p_T spectator jets substantially enhances the signal/background ratio, such double tagging proves to be too costly to the signal [10-13]. It has been recently suggested that tagging just one of these quarks as a single *energetic* jet can be just as efficient in suppressing the backgrounds that do not intrinsically require spectator jets, and far more efficient in retaining the signal for a heavy Higgs boson [13-15]. Thus, to isolate the heavy Higgs and other types of strong W_LW_L signals, we will apply such a forward jet-tag for most final state channels [13-17].

The detailed characteristics of W_L emission and the associated spectator jets also play a role in separating W_LW_L scattering from the background processes which *do* yield spectator jets (as well as two W's) in the final state. The crucial point to note is that the initial W_L's participating in the W_LW_L scattering have a $1/(p_T^2 + M_W^2)^2$ distribution with respect to the quarks from which they are emitted. This is to be contrasted, for instance, with W_TW_T scattering where the initiating W_T's have a $p_T^2/(p_T^2 + M_W^2)^2$ distribution with respect to the emitting quarks. The softer p_T distribution in the W_LW_L case has two primary consequences. First, the final W_LW_L pair is likely to have much more limited net transverse motion than W_LW_T and W_TW_T pairs produced through the various irreducible backgrounds.

Secondly, the spectator quarks left behind tend to emerge with smaller p_T (order of $M_W/2$), and correspondingly larger rapidity, than those associated with the background processes containing spectator jets and W_LW_T or W_TW_T pairs.

There are several crucial secondary consequences resulting from the above special characteristics of W_LW_L scattering. First, as discussed above, the jets from the gluon-exchange background and the electroweak background are generally harder and more central than those from the signal [12,16]. Therefore we will normally veto hard central jets to enhance the signal/background ratio [12,16,17]. Such a veto retains most of the signal events. As a further bonus, a central jet-veto is especially effective in suppressing the reducible background from heavy quark production and decay. The jets associated with this latter type of background populate a much more central region than do those from spectator quarks. Another consequence of the small p_T of the W_LW_L system is that we expect the charged leptons from the decays of the two final W_L's to be very back-to-back in the transverse plane [16,17]. This is due not only to the limited p_T of the W_LW_L system but also to the fact that the bulk of the leptons emitted from each final W_L will have a significant (and relatively similar) fraction of the W_L's total momentum. The latter fact also implies that the leptons will generally be very energetic. A cut requiring that the leptons appearing in the final state be very energetic and very back-to-back will substantially reduce all backgrounds, while being highly efficient in retaining the W_LW_L signal events.

We have already noted that the charged leptons will be required to be isolated. In order to completely eliminate the background from heavy quark production and decay (say, b or c semileptonic decays) in all channels, we implicitly assume that it will be possible to implement an isolation requirement according to which the hadronic energy deposit within a cone $\Delta R < 0.3$ around the lepton must be less than about 5 GeV [18].

Before proceeding, we wish to reemphasize the precise definition of the signal and background that we employ. The results in this section will all be based on the full matrix element calculations for the Standard Model. We define the heavy Higgs boson signal to be the difference between the cross section with a heavy Higgs boson and the result with a light Higgs; for example,

$$\sigma(\text{signal for a 1 TeV Higgs boson}) \;=\; \sigma(m_H = 1 \text{ TeV}) - \sigma(m_H = 100 \text{ GeV}) \;, \qquad (2.2)$$

where all W helicities have been included for both m_H values. At SSC energies, the EW rate for production of W pairs in which one or both of the W's is transversely polarized is essentially independent of the Higgs mass, while W_LW_L production is extremely small at $m_H = 100$ GeV. Thus, the prescription (2.2) measures the production rate of longitudinally polarized W bosons at large m_H. We will sometimes refer to this definition of the signal as the "subtraction" result.

As stated earlier in the introduction, we are only interested in the EW symmetry breaking sector; we do not include contributions to the W_LW_L final state arising from processes such

as $gg, q\bar{q} \rightarrow t\bar{t}H$ and $gg \rightarrow H$ (via a top quark loop) that depend upon the Yukawa couplings of the Higgs boson.

We now turn to a detailed discussion of the signals and backgrounds for the leptonic decay modes associated with each of the possible $W_L W_L$ scattering channels.

1) $W^+W^- \rightarrow ZZ, ZZ \rightarrow ZZ$

We first consider the "gold-plated" events with four charged leptons from ZZ decays. This gives a clean and distinct signal because the ZZ pairs can be fully reconstructed. The disadvantage is the rather small leptonic branching fraction, BR($ZZ \rightarrow 4\ell$) = 0.45%.

The major Standard Model backgrounds for this process arise from continuum ZZ production via tree-level processes at $\mathcal{O}(\alpha^2)$, $\mathcal{O}(\alpha^2\alpha_s)$ and $\mathcal{O}(\alpha^2\alpha_s^2)$ [19-21]; for example,

$$qq \rightarrow ZZ + \text{jets}\,, \tag{2.3}$$

which we will refer to as the QCD background. This set of backgrounds includes, in particular, diagrams at order $\alpha^2\alpha_s^2$ from gluon-exchange diagrams in which two quarks scatter via gluon exchange while two vector bosons are emitted from either the initial or final quark lines. Since the Z's are relatively weakly coupled to quark lines, this type of background is small in this case. At supercollider energies, the one-loop process

$$gg \rightarrow ZZ \tag{2.4}$$

is also not negligible. The total production rate is 30-70% as large as that from $q\bar{q} \rightarrow ZZ$, depending on the top quark mass [22]. However, we are interested in the large $M(ZZ)$ region, and require a very energetic jet in the final state, so the effective gluon luminosity is suppressed to a level where we can ignore gluon fusion in our calculations.

The $\mathcal{O}(\alpha^4)$ electroweak production of transversely polarized Z-pairs is another irreducible background [11,13,23]. Although it is formally higher-order than Eq. (2.3) in terms of the electroweak coupling constant, the kinematics are so similar to the signal that it must also be included. We will refer to this as the electroweak (EW) background.

In a recent study, kinematical cuts were developed to suppress these backgrounds for detecting a heavy SM Higgs boson at the SSC and the LHC [13]. We will use the same cuts,

$$\begin{aligned} p_T(\ell) &> 40 \text{ GeV}\,, \qquad |y(\ell)| < 2.5\,, \\ M(ZZ) &> 500 \text{ GeV}\,, \qquad p_T(Z) > \frac{1}{4}\sqrt{M(ZZ)^2 - 4M_Z^2}\,, \end{aligned} \tag{2.5}$$

where $y(\ell)$ is the rapidity of the lepton ℓ, and $M(ZZ)$ is the invariant mass of the two Z's in the final state. The transverse momentum cut on the Z's is motivated by its facility in removing the QCD background [24]. As discussed above, a forward (or backward) jet-tag

is very effective in suppressing the QCD and EW backgrounds [13]. Therefore, we will also require a tagged jet in the region

$$E(j_{\rm tag}) > 1.0\ (0.8)\ {\rm TeV}\ , \qquad 3 < |y(j_{\rm tag})| < 5\ , \qquad p_T(j_{\rm tag}) > 40\ {\rm GeV}\ , \tag{2.6}$$

where the number outside (inside) the parentheses refers to the cut applied at the SSC (LHC).

The jet-tagging efficiency is about 60% for the signal. The combined cuts essentially eliminate the QCD background and substantially suppress the EW background. An additional cut requiring the leptons from opposite Z's to be back-to-back is not needed in this case.

2) $W^+W^- \to W^+W^-, ZZ \to W^+W^-$

We next consider W^+W^- events in the $\ell\bar{\nu}_\ell\bar{\ell}\nu_\ell$ final state, where $\ell = e, \mu$. The leptonic branching fraction is ${\rm BR}(WW \to \ell\bar{\nu}_\ell\bar{\ell}\nu_\ell) = 4.7\%$, so we expect a larger number of events in this channel. Although the two W's cannot be fully reconstructed, any s-channel resonance, such as the Standard Model Higgs boson, significantly enhances the production rate, and the $M(\ell\ell)$ spectrum peaks broadly at about one-half the resonance mass [14].

Unfortunately, there are now reducible backgrounds besides the irreducible backgrounds from continuum QCD and EW processes. The most important ones are

$$q\bar{q}, gg \to t\bar{t}\ , \quad gg \to t\bar{t}g\ , \quad qg \to t\bar{t}q\ , \quad q\bar{q} \to t\bar{t}g\ , \tag{2.7}$$

where the top quarks decay into real W's [25-27].

To reduce the backgrounds, we first impose stringent leptonic cuts

$$\begin{aligned} p_T(\ell) &> 100\ {\rm GeV}\ , \qquad |y(\ell)| < 2\ , \\ \Delta p_T(\ell\ell) &\equiv |\mathbf{p_T}(\ell_1) - \mathbf{p_T}(\ell_2)| > 450\ {\rm GeV}\ , \\ M(\ell\ell) &> 250\ {\rm GeV}\ , \qquad \cos\phi_{\ell\ell} < -0.8\ , \end{aligned} \tag{2.8}$$

where $\Delta p_T(\ell\ell)$ and $\cos\phi_{\ell\ell}$ are, respectively, the difference of the transverse momenta and the cosine of the opening angle in the transverse plane of the two charged leptons. The cuts on these two variables are based on our earlier observations that the lepton-pair decay products are more energetic and more back-to-back in the transverse plane for signal events than for the backgrounds [16]. For example, the transverse momentum of the charged leptons, $p_T(\ell)$, for the signal will typically be of order $m_H/4$. For a 1 TeV Higgs boson, $\Delta p_T(\ell\ell) \sim m_H/2 = 500$ GeV.

We also impose the jet-tagging conditions [14]

$$E(j_{\rm tag}) > 1.5\ (1.0)\ {\rm TeV}\ , \qquad 3 < |y(j_{\rm tag})| < 5\ , \qquad p_T(j_{\rm tag}) > 40\ {\rm GeV}\ . \tag{2.9}$$

The $E(j_{\rm tag})$ cut has been made slightly more stringent than Eq. (2.6) in order to control the much larger $t\bar{t}g$ background. We further suppress the top background by a central jet-veto

in which events with jets with [14]

$$p_T(j_{\rm veto}) \ > \ 30 \ {\rm GeV} \ , \qquad |y(j_{\rm veto})| \ < 3 \tag{2.10}$$

are rejected. In Ref. 29, a central jet threshold of 25 GeV was used by the SDC collaboration. Our choice in Eq. (2.10) is slightly more conservative.

Combining the cuts of Eqs. (2.8)-(2.10), we can reduce the backgrounds below the $W_L^+W_L^-$ signal. Especially significant is the effective reduction of the large $t\bar{t}$ background. With the leptonic cuts of Eq. (2.8) imposed, the overall efficiency for jet-tagging and vetoing is about 38% for the signal. We have chosen $m_t = 140$ GeV as representative in our background analyses throughout this paper. If the top quark is heavier, our jet-veto cut would be more effective and the $t\bar{t}j$ background would be easier to separate [14].

3) $W^+Z \ \to \ W^+Z$

We now turn to the WZ events with $\ell\bar{\nu}_\ell\ell\bar{\ell}$ final states. The leptonic branching fraction is ${\rm BR}(W^+Z \to \ell\bar{\nu}_\ell\ell\bar{\ell}) = 1.5\%$.

For this channel, we choose the leptonic acceptance cuts as follows,

$$\begin{aligned} p_T(\ell) \ &> 40 \ {\rm GeV} \ , \qquad |y(\ell)| \ < \ 2.5 \ , \\ \not{p}_T \ &> 75 \ {\rm GeV} \ , \qquad M_T \ > \ 500 \ {\rm GeV} \ , \ p_T(Z) \ > \ \frac{1}{4}M_T \ , \end{aligned} \tag{2.11}$$

where $\not{p}_T$ denotes the missing transverse momentum and M_T is the cluster transverse mass of the WZ system, defined by [28]

$$M_T^2 \ = \ \left(\sqrt{M^2(\ell\ell\ell) + p_T^2(\ell\ell\ell)} + |\not{p}_T|\right)^2 - ({\bf p}_T(\ell\ell\ell) + \not{\bf p}_T)^2 \ . \tag{2.12}$$

Analogous to the cut on $p_T(Z)$ given in Eq. (2.5), the $p_T(Z)$ cut in Eq. (2.11) is useful for removing the QCD background.

To reduce the QCD and EW backgrounds, following Ref. 15, we tag a jet with

$$E(j_{\rm tag}) \ > \ 2.0 \ (1.5) \ {\rm TeV} \ , \qquad 3 \ < \ |y(j_{\rm tag})| \ < \ 5 \ , \ p_T(j_{\rm tag}) \ > \ 40 \ {\rm GeV} \ . \tag{2.13}$$

We can reduce the background from Z and top quark associated production,

$$q\bar{q}, gg \ \to \ Zt\bar{t} \ , \tag{2.14}$$

by imposing the jet-vetoing of Eq. (2.10).

The tagging plus vetoing efficiency is about 40% for the signal. As for the fully reconstructable $ZZ \to 4\ell$ mode, a back-to-back lepton cut is not needed here.

4) $W^+W^+ \to W^+W^+$

Finally, we discuss the like-sign W process with two like-sign charged leptons in the final state [30,12,16,31,17]. This mode is attractive because of the distinctive final state and absence of an order α^2 continuum background.

However, backgrounds to the $W_L^+W_L^+$ signal do exist. Besides the transversely polarized background from EW processes, there is the previously-mentioned background contributing at order $\alpha^2\alpha_s^2$,

$$qq \to qqW^+W^+ \ , \tag{2.15}$$

in which a gluon is exchanged between the scattering quarks [8,32]. Since there is no lowest order (α^2 or $\alpha^2\alpha_s$) background, this process is potentially significant for this channel. Finally, there is a background from associated $Wt\bar{t}$ production [12],

$$q'\bar{q} \to Wt\bar{t} \ , \tag{2.16}$$

with $t \to W^+b$.

We first impose the leptonic cuts of Eq. (2.8), with the exception of a weaker cut $\Delta p_T(\ell\ell) > 200$ GeV. The back-to-back cuts are advantageous in the present channel [16,17]. We also apply the jet-vetoing of Eq. (2.10) to this case, with a looser cut $p_T(j_{\rm veto}) > 60$ GeV [12], and find that it greatly reduces the backgrounds.

Another potentially large background is that from $t\bar{t}$ production with a cascade decay, $\bar{t} \to \bar{b}W^- \to \ell^+X$. However, the ℓ^+ from the $\bar{b}$ decay is usually not isolated. When the ℓ^+ is fast, the other hadrons from the $\bar{b}$ decay tend to be collinear with the ℓ^+. The lepton isolation requirement that we have implicitly assumed should be able to eliminate this cascade decay background [17,18].

With the leptonic cuts imposed, the jet-vetoing efficiency for this signal is about 70%.

Jet-tagging can also be applied to the W^+W^+ process [16,17]. By tagging a forward jet and imposing a cut on the minimum invariant mass of the tagged jet and a lepton, $M(\ell j_{\rm tag}) > 200$ GeV, it is possible to further reduce the backgrounds. This tag is especially effective to reduce the $t\bar{t}$ cascade decay background since $M(\ell j_{\rm tag})$ is significantly larger for the signal than for the background. However, since we assume that charged lepton isolation can be implemented at the level required to eliminate the cascade decay background, we will not impose such a cut in this paper. Should a problem arise in experimentally implementing lepton isolation, this type of cut can be used as an alternative.

In Table 1 we list the kinematic cuts used in our study at the SSC (and LHC in parentheses). In Tables 2a and 2b we present the cross sections obtained in the SM from the electroweak processes at $m_H = 1$ TeV and at $m_H = 0.1$ TeV, as well as those for the $q\bar{q}$ annihilation continuum pair production (QCD) reactions. The results in the "leptonic cuts

Table 1: Leptonic cuts, tagging and vetoing cuts on jets, by mode at the SSC (LHC).

ZZ leptonic cuts	Tag only
$\|y(\ell)\| < 2.5$	$E(j_{tag}) > 1.0$ (0.8) TeV
$p_T(\ell) > 40$ GeV	$3.0 < \|y(j_{tag})\| < 5.0$
$p_T(Z) > \frac{1}{4}\sqrt{M^2(ZZ) - 4M_Z^2}$	$p_T(j_{tag}) > 40$ GeV
$M(ZZ) > 500$ GeV	
W^+W^- leptonic cuts	Tag and Veto
$\|y(\ell)\| < 2.0$	$E(j_{tag}) > 1.5$ (1.0) TeV
$p_T(\ell) > 100$ GeV	$3.0 < \|y(j_{tag})\| < 5.0$
$\Delta p_T(\ell\ell) > 450$ GeV	$p_T(j_{tag}) > 40$ GeV
$\cos\phi_{\ell\ell} < -0.8$	$p_T(j_{veto}) > 30$ GeV
$M(\ell\ell) > 250$ GeV	$\|y(j_{veto})\| < 3.0$
W^+Z leptonic cuts	Tag and Veto
$\|y(\ell)\| < 2.5$	$E(j_{tag}) > 2.0$ (1.5) TeV
$p_T(\ell) > 40$ GeV	$3.0 < \|y(j_{tag})\| < 5.0$
$\not{p}_T > 75$ GeV	$p_T(j_{tag}) > 40$ GeV
$p_T(Z) > \frac{1}{4}M_T$	$p_T(j_{veto}) > 60$ GeV
$M_T > 500$ GeV	$\|y(j_{veto})\| < 3.0$
W^+W^+ leptonic cuts	Veto only
$\|y(\ell)\| < 2.0$	$p_T(j_{veto}) > 60$ GeV
$p_T(\ell) > 100$ GeV	$\|y(j_{veto})\| < 3.0$
$\Delta p_T(\ell\ell) > 200$ GeV	
$\cos\phi_{\ell\ell} < -0.8$	
$M(\ell\ell) > 250$ GeV	

only" column are those obtained by imposing only the leptonic cuts of Table 1, including the back-to-back cuts in the W^+W^- and $W^\pm W^\pm$ channels. In the next two columns, the cross sections obtained after imposing jet-tagging and/or vetoing, *in addition to the leptonic cuts*, are given. The efficiencies at the SSC and LHC for the signal are obtained by taking the difference between the $m_H = 1$ TeV and $m_H = 0.1$ TeV results. The branching ratios for each leptonic channel and the efficiencies for the signal when performing jet-tagging and/or vetoing (with leptonic cuts already imposed) are summarized in Table 3.

For other models of W_LW_L interactions, we will proceed as follows. We first compute the cross sections for W_LW_L production in a given model by using the Effective W Approximation (EWA) [4,5] and the Equivalence Theorem (ET) [1-3]. In using the EWA we compute

Table 2a: Standard Model cross sections (in fb) for $m_H = 1$ TeV, $m_H = 0.1$ TeV, and for the QCD background, with $\sqrt{s} = 40$ TeV, $m_t = 140$ GeV.

ZZ	leptonic cuts only	tag only	veto plus tag
$EW(m_H = 1\ TeV)$	1.2	0.68	-
$EW(m_H = 0.1\ TeV)$	0.17	0.07	-
QCD	0.92	0.02	-
W^+W^-	leptonic cuts only	veto only	veto plus tag
$EW(m_H = 1\ TeV)$	11	5.5	3.6
$EW(m_H = 0.1\ TeV)$	2.2	0.49	0.30
QCD	15	15	0.31
$t\bar{t}j$	1300	14	1.5
W^+Z	leptonic cuts only	veto only	veto plus tag
$EW(m_H = 1\ TeV)$	1.3	0.41	0.21
$EW(m_H = 0.1\ TeV)$	1.1	0.26	0.13
QCD	3.1	3.1	0.11
$Zt\bar{t}j$	1.4	0.04	0.01
W^+W^+	leptonic cuts only	veto only	veto plus tag
$EW(m_H = 1\ TeV)$	2.4	0.98	-
$EW(m_H = 0.1\ TeV)$	1.4	0.29	-
QCD	0.24	0.01	-
$Wt\bar{t}$	0.75	0.05	-

total cross sections ignoring all jet observables. To assess the inaccuracies that might arise as a result of these approximations, we will make a detailed comparison between the EWA and ET computations and the exact SM calculation in section 4. To implement the lepton cuts, including back-to-back requirements in the W^+W^- and $W^\pm W^\pm$ channels, we decay the final W_L's according to the appropriate angular distributions. The results will differ from the exact calculation to the extent that lepton cut efficiencies depend upon the p_T of the WW system. For the cuts employed, a comparison between the exact and EWA lepton cut efficiencies is made in section 4 for the 1 TeV SM Higgs case, and good agreement is found. To obtain cross sections in the EWA approximation that include the jet-tagging and jet-vetoing cuts, we will simply multiply the cross sections calculated from EWA by the net jet-tagging and/or jet-vetoing efficiency for each channel as computed for the W_LW_L signal in the exact SM calculation with a 1 TeV Higgs boson. We believe that this procedure should be fairly accurate. Indeed, the kinematics of the jets in the signal events are determined by the kinematics of the initial W_L's that participate in the W_LW_L scattering process. These

Table 2b: Standard Model cross sections (in fb) for $m_H = 1$ TeV, $m_H = 0.1$ TeV, and for the QCD background, with $\sqrt{s} = 16$ TeV, $m_t = 140$ GeV.

ZZ	leptonic cuts only	tag only	veto plus tag
$EW(m_H = 1\ TeV)$	0.17	0.076	-
$EW(m_H = 0.1\ TeV)$	0.029	0.007	-
QCD	0.33	0.003	-
W^+W^-	leptonic cuts only	veto only	veto plus tag
$EW(m_H = 1\ TeV)$	1.6	0.52	0.31
$EW(m_H = 0.1\ TeV)$	0.42	0.049	0.022
QCD	4.3	4.3	0.042
$t\bar{t}j$	107	1.5	0.12
W^+Z	leptonic cuts only	veto only	veto plus tag
$EW(m_H = 1\ TeV)$	0.25	0.059	0.022
$EW(m_H = 0.1\ TeV)$	0.20	0.035	0.012
QCD	1.2	1.2	0.011
$Zt\bar{t}j$	0.085	0.003	0.000
W^+W^+	leptonic cuts only	veto only	veto plus tag
$EW(m_H = 1\ TeV)$	0.43	0.13	-
$EW(m_H = 0.1\ TeV)$	0.27	0.037	-
QCD	0.063	0.003	-
$Wt\bar{t}$	0.24	0.02	-

Table 3: WW leptonic branching ratios, and the efficiencies of jet-tagging and vetoing for the W_LW_L signal at the SSC (LHC).

ZZ	branching ratio	tag only	veto plus tag
	0.45%	59% (49%)	-
W^+W^-	branching ratio	veto only	veto plus tag
	4.7%	57% (40%)	38% (24%)
W^+Z	branching ratio	veto only	veto plus tag
	1.5%	75% (48%)	40% (20%)
W^+W^+	branching ratio	veto only	veto plus tag
	4.7%	69% (58%)	-

kinematics are independent of the strong $W_L W_L$ scattering amplitude.

3. Beyond the Standard Model

In this section we present a variety of models that unitarize the $W_L W_L$ scattering amplitude. We start by reviewing the Standard Model, and then discuss other possibilities that are consistent with all the data to date [33].

Let us begin by recalling that in the Standard Model, the $W_L W_L$ scattering amplitudes are unitarized by exchange of a spin-zero resonance, the Higgs particle H. The Higgs boson is contained in a complex scalar doublet,

$$\Phi \;=\; (v+H)\exp(2iw^a\tau^a/v)\;, \tag{3.1}$$

where the τ^a are the generators of $SU(2)$, normalized so that $\mathrm{Tr}\,\tau^a\tau^b = \delta^{ab}/2$. The four components of Φ contain three would-be Goldstone bosons w^a and the Higgs particle H. In the Standard Model, the Higgs potential,

$$\mathcal{V} \;=\; \frac{\lambda}{16}\left[\mathrm{Tr}\left(\Phi^\dagger\Phi - v^2\right)\right]^2, \tag{3.2}$$

is invariant under a rigid $SU(2)_L \times SU(2)_R$ symmetry,

$$\Phi \;\rightarrow\; L\,\Phi\,R^\dagger\;, \tag{3.3}$$

with $L, R \in SU(2)$. The vacuum expectation value

$$\langle\Phi\rangle \;=\; v\;, \tag{3.4}$$

breaks the symmetry to the diagonal $SU(2)$. In the perturbative limit, it also gives mass to the Higgs boson,

$$m_H \;=\; \sqrt{2\lambda}\,v\;, \tag{3.5}$$

where $v = 246$ GeV.

In the Standard Model, the diagonal $SU(2)$ symmetry is broken only by terms proportional to the hypercharge coupling g' and the up-down fermion mass splittings. It is responsible for the successful mass relation

$$M_W \;=\; M_Z\,\cos\theta\;, \tag{3.6}$$

where θ is the weak mixing angle; M_W and M_Z are the masses of $W^\pm$ and Z, respectively. The four components of Φ split into a triplet w^a and a singlet H under the $SU(2)$ symmetry. In analogy to the chiral symmetry of QCD, we call the unbroken $SU(2)$ "isospin."

At high energies, the scattering of longitudinally polarized W particles can be approximated by the scattering of the would-be Goldstone bosons w^a [1-3]. For the Standard Model, this is a calculational simplification, but for other models it is a powerful conceptual aid as well. For example, if one thinks of the would-be Goldstone fields in analogy with the pions of QCD, one expects the $W_L W_L$ scattering amplitudes to be unitarized by a spin-one, isospin-one vector resonance, like the techni-rho. Alternatively, if one thinks of the Goldstone fields in terms of the linear sigma model, one expects the scattering amplitudes to be unitarized by a spin-zero, isospin-zero scalar field like the Higgs boson.

In this paper, we are interested in the strongly interacting longitudinal W's in the TeV region. We will ignore the gauge couplings and the up-down fermion mass splittings. Therefore, the SU(2) "isospin" is conserved. The $W_L W_L$ scattering amplitudes can then be written in terms of isospin amplitudes, exactly as in QCD. If we assign isospin indices as follows,

$$W_L^a \, W_L^b \;\to\; W_L^c \, W_L^d \;, \tag{3.7}$$

then the scattering amplitude is given by

$$\mathcal{M}(W_L^a W_L^b \to W_L^c W_L^d) \;=\; A(s,t,u)\delta^{ab}\delta^{cd} \;+\; A(t,s,u)\delta^{ac}\delta^{bd} \;+\; A(u,t,s)\delta^{ad}\delta^{bc} \;, \tag{3.8}$$

where $a,b,c,d = 1,2,3$. (We use W_L to denote either $W_L^\pm$ or Z_L, where $W_L^\pm = (1/\sqrt{2})(W_L^1 \mp iW_L^2)$ and $Z_L = W_L^3$.) All the physics of $W_L W_L$ scattering is contained in the amplitude functions A.

Given the amplitude functions, the physical amplitudes for boson-boson scattering are given as follows,

$$\begin{aligned}
\mathcal{M}(W_L^+ W_L^- \to Z_L Z_L) &= A(s,t,u) \\
\mathcal{M}(Z_L Z_L \to W_L^+ W_L^-) &= A(s,t,u) \\
\mathcal{M}(W_L^+ W_L^- \to W_L^+ W_L^-) &= A(s,t,u) \;+\; A(t,s,u) \\
\mathcal{M}(Z_L Z_L \to Z_L Z_L) &= A(s,t,u) \;+\; A(t,s,u) \;+\; A(u,t,s) \\
\mathcal{M}(W_L^\pm Z_L \to W_L^\pm Z_L) &= A(t,s,u) \\
\mathcal{M}(W_L^\pm W_L^\pm \to W_L^\pm W_L^\pm) &= A(t,s,u) \;+\; A(u,t,s) \;.
\end{aligned} \tag{3.9}$$

In these expressions, the amplitudes do not include the symmetry factors for identical particles.

The isospin amplitudes $T(I)$, for isospin I, are given by

$$\begin{aligned}
T(0) &= 3\,A(s,t,u) \;+\; A(t,s,u) \;+\; A(u,t,s) \\
T(1) &= A(t,s,u) \;-\; A(u,t,s) \\
T(2) &= A(t,s,u) \;+\; A(u,t,s) \;.
\end{aligned} \tag{3.10}$$

In terms of the isospin amplitudes, the physical scattering amplitudes can be written

$$\begin{aligned}
\mathcal{M}(W_L^+W_L^- \to Z_LZ_L) &= \frac{1}{3}[T(0) - T(2)] \\
\mathcal{M}(Z_LZ_L \to W_L^+W_L^-) &= \frac{1}{3}[T(0) - T(2)] \\
\mathcal{M}(W_L^+W_L^- \to W_L^+W_L^-) &= \frac{1}{6}[2T(0) + 3T(1) + T(2)] \\
\mathcal{M}(Z_LZ_L \to Z_LZ_L) &= \frac{1}{3}[T(0) + 2T(2)] \\
\mathcal{M}(W_L^\pm Z_L \to W_L^\pm Z_L) &= \frac{1}{2}[T(1) + T(2)] \\
\mathcal{M}(W_L^\pm W_L^\pm \to W_L^\pm W_L^\pm) &= T(2) \, .
\end{aligned} \tag{3.11}$$

Again, these amplitudes do not include the symmetry factors for identical particles.

For the Standard Model, the amplitude functions are easy to work out. They can be expressed by

$$A(s,t,u) = \frac{-m_H^2}{v^2}\left(1 + \frac{m_H^2}{s - m_H^2 + im_H\Gamma_H\theta(s)}\right) , \tag{3.12}$$

where m_H and $\Gamma_H = 3m_H^3/32\pi v^2$ are the mass and width of the Higgs boson; $\theta(s)$ is the step-function which takes the value one for $s > 0$ and zero otherwise. Note that we have included a Breit-Wigner width for the Higgs particle in the s-channel. This is a violation of the equivalence theorem, which causes an increase in the rate in the resonant channels [34-36]. More discussion of this violation will appear later. We have not included the width in the non-resonant channels.

The Standard Model has the advantage that it is a renormalizable theory, and that all amplitudes are perturbatively unitary so long as m_H is not too large. Of course, at $m_H = 1$ TeV, some small amount of unitarity violation occurs near the resonance. Nonetheless, the signal rates we obtain for $m_H = 1$ TeV provide a first characterization of what one might expect in the case where W_LW_L interactions become strong.

There are many other models that provide alternative descriptions of electroweak symmetry breaking. (We shall only consider models without any open inelastic channels in W_LW_L scattering.) Many of these models are effective theories, based on nonrenormalizable chiral lagrangians for the WW sector. These models must be understood in the context of an energy expansion. Generally, such an expansion does not provide a unitary description for all energies. This is simply because the effective lagrangian does not make explicit the new physics that must appear at some scale Λ, well above the WW mass region where it is to be employed. For the purposes of this paper, we must ensure that the effective theories are unitary for the WW masses of interest.

To check unitarity, we first write the scattering amplitudes in terms of the isospin amplitudes $T(I)$. We then expand in partial waves according to the usual formula

$$\begin{aligned} T(I) &= 32\pi \sum_{\ell=0}^{\infty} (2\ell+1) P_\ell(\cos\theta) a_\ell^I \ , \\ a_\ell^I &= \frac{1}{64\pi} \int_{-1}^{1} d(\cos\theta) P_\ell(\cos\theta) T(I) \ . \end{aligned} \tag{3.13}$$

Two-body elastic unitarity is equivalent to the statement $|a_\ell^I - i/2| = 1/2$. In this paper we will require $\mathrm{Re}\, a_\ell^I < 1/2$ as our unitarity condition.

Among possible alternative models, there are several distinctions we can make. The first is whether or not a particular model is resonant in the $W_L W_L$ channel. If it is resonant, the model can be classified by the spin and isospin of the resonance. If it is not, the analysis is more subtle. Nonetheless, we shall see that all possibilities can be described in terms of two parameters. In this work, we will restrict our attention to models with spin-zero, isospin-zero resonances (like the Higgs boson), and spin-one, isospin-one resonances (like the techni-rho resonance), and nonresonant models.

3.1. Spin-zero, Isospin-zero Resonances

3.1.1 The $O(2N)$ Model

The first model we discuss represents an attempt to describe the Standard Model Higgs in the nonperturbative domain. In the perturbatively-coupled Standard Model, the mass of the Higgs is proportional to the square root of the scalar self-coupling λ. Heavy Higgs particles correspond to large values of λ. For $m_H \gtrsim 1$ TeV, naive perturbation theory breaks down, and one must take a more sophisticated approach.

One possibility for exploring the nonperturbative regime is to exploit the isomorphism between $SU(2)_L \times SU(2)_R$ and $O(4)$ [37]. Using a large-N approximation, one can solve the $O(2N)$ model for all values of λ, to leading order in $1/N$. The resulting scattering amplitudes can be parameterized by the scale Λ of the Landau pole. Large values of Λ correspond to small couplings λ and relatively light Higgs particles. In contrast, small values of Λ correspond to large λ and describe the nonperturbative regime.

The amplitude functions can be found via standard large-N techniques. In the limit $N \to \infty$, they are [38]

$$A(s,t,u) = \frac{16\pi^2 s}{16\pi^2 v^2 - sN[2 + \ln(\Lambda^2/|s|) + i\pi\theta(s)]} \ , \tag{3.14}$$

where Λ is the physical cutoff and $\theta(s)$ is the step-function defined below Eq. (3.12). The scale of the cutoff completely determines the theory.

It is not hard to show that the $W_L W_L$ scattering amplitudes respect the unitarity condition for all energies $E \lesssim \Lambda$. In this paper we will take $N = 2$ and $\Lambda = 3$ TeV to characterize the strongly-coupled Standard Model. If we parameterize the position of the pole by its "mass" m and "width" Γ through the relation $s = (m - \frac{i}{2}\Gamma)^2$, then $m \sim 0.8$ TeV and $\Gamma \sim 600$ GeV.

3.1.2 The Chirally-Coupled Scalar Model

The second model describes the low-energy regime of a technicolor-like model whose lowest resonance is a techni-sigma. The effective lagrangian for such a resonance can be constructed using the techniques of Callan, Coleman, Wess and Zumino [39]. The resulting lagrangian is consistent with the chiral symmetry $SU(2)_L \times SU(2)_R$, spontaneously broken to the diagonal $SU(2)$.

In this approach, the basic fields are $\Sigma = \exp(2iw^a\tau^a/v)$ and a scalar S. These fields transform as follows under $SU(2)_L \times SU(2)_R$,

$$\begin{aligned} \Sigma &\to L\,\Sigma\,R^\dagger\,, \\ S &\to S\,. \end{aligned} \tag{3.15}$$

This is all we need to construct the effective lagrangian. To the order of interest, it is given by

$$\begin{aligned} \mathcal{L}_{\text{Scalar}} &= \frac{v^2}{4}\,\mathrm{Tr}\,\partial^\mu\Sigma^\dagger\partial_\mu\Sigma \\ &+ \frac{1}{2}\,\partial^\mu S\partial_\mu S - \frac{1}{2}\,M_S^2\,S^2 \\ &+ \frac{1}{2}\,gv\,S\,\mathrm{Tr}\,\partial^\mu\Sigma^\dagger\partial_\mu\Sigma + \ldots\,, \end{aligned} \tag{3.16}$$

where M_S is the isoscalar mass, and g is related to its partial width into the Goldstone fields,

$$\Gamma_S = \frac{3g^2M_S^3}{32\pi v^2}\,. \tag{3.17}$$

To this order, the lagrangian (3.16) is the most general chirally-symmetric coupling of a spin-zero isoscalar resonance to the fields w^a. It contains two free parameters, which can be traded for the mass and the width of the S. For $g = 1$, the S reduces to an ordinary Higgs. For $g \neq 1$, however, the S is *not* a typical Higgs. It is simply an isoscalar resonance of arbitrary mass and width. In either case, one must be sure to check that the scattering amplitudes are unitary up to the energy of interest.

The tree-level scattering amplitude is easy to construct. It has two terms. The first is a direct four-Goldstone coupling which ensures that the scattering amplitude satisfies the

Low-Energy Theorems (LET) [40]. The second contains the contributions from the isoscalar resonance. Taken together, they give the full scattering amplitude,

$$A(s,t,u) \;=\; \frac{s}{v^2} \;-\; \left(\frac{g^2 s^2}{v^2}\right) \frac{1}{s - M_S^2 + i M_S \Gamma_S \theta(s)} \;. \tag{3.18}$$

In what follows, we will choose $M_S = 1.0$ TeV, $\Gamma_S = 350$ GeV. These values give unitary scattering amplitudes up to 2 TeV. (We use the Breit–Wigner prescription to handle the s–channel resonance. Our criteria is to have all the partial waves respect the unitarity condition up to 2 TeV except near the resonance; the slight unitarity violation near the resonance is due to the perturbative expansion of the width [34-36].)

3.2. Spin-one, Isospin-one Resonances

3.2.1 The Chirally Coupled Vector Model

This example provides a relatively model-independent description of the techni-rho resonance that arises in most technicolor theories. As above, one can use the techniques of nonlinear realizations to construct the most general coupling consistent with chiral symmetry [39,41-43].

To find the techni-rho lagrangian, we first parameterize the Goldstone fields w^a in a slightly different way,

$$\xi \;=\; \exp(i w^a \tau^a / v) \;, \tag{3.19}$$

so $\Sigma = \xi^2$. We then represent an $SU(2)_L \times SU(2)_R$ transformation on the field ξ as follows:

$$\xi \;\to\; \xi' \;\equiv\; L \xi U^\dagger \;=\; U \xi R^\dagger \;. \tag{3.20}$$

Here L, R and U are $SU(2)$ group elements, and U is a (nonlinear) function of L, R and w^a, chosen to restore ξ' to the form (3.19). Note that when $L = R$, $U = L = R$ and the transformation linearizes. This simply says that the w^a transform as a triplet under the diagonal $SU(2)$.

Given these transformations, one can construct the following currents,

$$\begin{aligned} J_{\mu L} \;&=\; \xi^\dagger \partial_\mu \xi \;\to\; U J_{\mu L} U^\dagger \;+\; U \partial_\mu U^\dagger \;, \\ J_{\mu R} \;&=\; \xi \partial_\mu \xi^\dagger \;\to\; U J_{\mu R} U^\dagger \;+\; U \partial_\mu U^\dagger \;. \end{aligned} \tag{3.21}$$

The currents $J_{\mu L}$ and $J_{\mu R}$ transform as gauge fields under transformations in the diagonal $SU(2)$. As above, the transformations linearize when $L = R = U$.

The transformations (3.21) inspire us to choose the techni-rho transformation as follows,

$$V_\mu \;\to\; U V_\mu U^\dagger \;+\; i g^{-1} U \partial_\mu U^\dagger \;. \tag{3.22}$$

In this expression, $V_\mu = V_\mu^a \tau^a$, and g is the techni-rho coupling constant. When $L = R = U$, Eq. (3.22) implies that the techni-rho transforms as an isotriplet of weak isospin.

Using these transformations, it is easy to construct the most general lagrangian consistent with chiral symmetry. We first write down the currents

$$\begin{aligned} \mathcal{A}_\mu &= J_{\mu L} - J_{\mu R} , \\ \mathcal{V}_\mu &= J_{\mu L} + J_{\mu R} + 2igV_\mu , \end{aligned} \tag{3.23}$$

which transform as follows under an arbitrary chiral transformation,

$$\begin{aligned} \mathcal{A}_\mu &\to U\mathcal{A}_\mu U^\dagger , \\ \mathcal{V}_\mu &\to U\mathcal{V}_\mu U^\dagger . \end{aligned} \tag{3.24}$$

Under parity (which exchanges J_L with J_R and leaves V invariant), $\mathcal{V}$ is invariant, while $\mathcal{A}$ changes sign. If we make the additional assumption that the underlying dynamics conserve parity, we are led to the following lagrangian,

$$\mathcal{L}_{\text{Vector}} = -\frac{1}{4} V^a_{\mu\nu} V^{a\mu\nu} - \frac{1}{4} v^2 \,\text{Tr}\, \mathcal{A}_\mu \mathcal{A}^\mu - \frac{1}{4} a v^2 \,\text{Tr}\, \mathcal{V}_\mu \mathcal{V}^\mu + \ldots , \tag{3.25}$$

where $V^a_{\mu\nu}$ is the (nonabelian) field-strength for the vector field V^a_μ. The dots in this equation denote terms with more derivatives. Up to a possible field redefinition, this is the most general coupling of a techni-rho resonance to the Goldstone bosons, consistent with $SU(2)_L \times SU(2)_R$ symmetry.

In this lagrangian, the parameter v is fixed as before. The parameters g and a, however, are free. One combination is determined by the mass of the techni-rho,

$$M_V^2 = a g^2 v^2 , \tag{3.26}$$

and another by its width into techni-pions (*i.e.* Goldstone bosons),

$$\Gamma_V = \frac{a M_V^3}{192\pi v^2} . \tag{3.27}$$

Because of the chiral symmetry, these two parameters completely define the theory.

As above, the scattering amplitude is easy to compute. It contains a direct four-Goldstone-boson coupling, as well as the isovector resonance. One finds

$$\begin{aligned} A(s,t,u) = \frac{s}{4v^2}\left(4 - 3\,a\right) + \frac{a M_V^2}{4v^2}\Bigg[&\frac{u-s}{t - M_V^2 + i M_V \Gamma_V \theta(t)} \\ &+ \frac{t-s}{u - M_V^2 + i M_V \Gamma_V \theta(u)}\Bigg] . \end{aligned} \tag{3.28}$$

In what follows we will choose $M_\rho = 2.0$ TeV, $\Gamma_\rho = 700$ GeV and $M_\rho = 2.5$ TeV, $\Gamma_\rho = 1300$ GeV. These values preserve unitarity up to 3 TeV, except for a small unitarity violation near the s-channel resonance in the a_1^1 partial wave. Additional constraints can be found from precision measurements of the electroweak parameters. Our choices are consistent with current limits [43].

3.3. NONRESONANT MODELS

Effective field theories provide a useful formalism for describing resonances in $W_L W_L$ scattering beyond the Standard Model. They also can be used to describe nonresonant models in which the $W_L W_L$ scattering occurs below the threshold for resonance production. The effective lagrangian description allows one to construct scattering amplitudes that are consistent with crossing, unitarity and chiral symmetry [44].

The most important effects at SSC energies can be found by considering the lagrangian for the Goldstone fields,

$$\begin{aligned} \mathcal{L}_{\text{Goldstone}} &= \frac{v^2}{4} \operatorname{Tr} \partial_\mu \Sigma^\dagger \partial^\mu \Sigma \\ &+ L_1 \left(\frac{v}{\Lambda}\right)^2 \operatorname{Tr}(\partial_\mu \Sigma^\dagger \partial^\mu \Sigma) \operatorname{Tr}(\partial_\nu \Sigma^\dagger \partial^\nu \Sigma) \\ &+ L_2 \left(\frac{v}{\Lambda}\right)^2 \operatorname{Tr}(\partial_\mu \Sigma^\dagger \partial_\nu \Sigma) \operatorname{Tr}(\partial^\mu \Sigma^\dagger \partial^\nu \Sigma) , \end{aligned} \tag{3.29}$$

where $\Lambda \lesssim 4\pi v$ denotes the scale of the new physics. To this order, this is the most general $SU(2)_L \times SU(2)_R$ invariant lagrangian for the Goldstone fields [45,46].

The lagrangian (3.29) describes new physics at energies below the mass of lightest new particles. All the effects of the new physics are contained in the coefficients of the higher-dimensional operators built from the Goldstone fields. To order p^2 in the energy expansion, only one operator contributes, and its coefficient is universal. To order p^4, however, there are two additional operators that contribute to $W_L W_L$ scattering.

To order p^4, the scattering amplitudes are given by

$$\begin{aligned} A(s,t,u) &= \frac{s}{v^2} + \frac{1}{4\pi^2 v^4}\left(2L_1(\mu)s^2 + L_2(\mu)(t^2+u^2)\right) \\ &+ \frac{1}{16\pi^2 v^4}\left[-\frac{t}{6}(s+2t)\log\left(-\frac{t}{\mu^2}\right) - \frac{u}{6}(s+2u)\log\left(-\frac{u}{\mu^2}\right)\right. \\ &\left. - \frac{s^2}{2}\log\left(-\frac{s}{\mu^2}\right)\right] , \end{aligned} \tag{3.30}$$

where we have taken $\Lambda = 4\pi v \sim 3.1$ TeV and the $L_i(\mu)$ are the renormalized coefficients in the effective lagrangian. ($\log(-s) = \log(s) - i\pi$, for $s > 0$.) To this order, there are two types of contributions. The first is a direct coupling that follows from the tree-level lagrangian. The second is a one-loop correction that must be included at order p^4. The loop contribution renormalizes the parameters L_1 and L_2, and gives finite logarithmic corrections that cannot be absorbed into a redefinition of the couplings.

The difficulty with this approach is that at SSC energies, the scattering amplitudes violate unitarity between 1 and 2 TeV. This indicates that new physics is near, but there is no guarantee that new resonances lie within the reach of the SSC. We choose to treat the uncertainties of unitarization in three ways:

1) We take $L_1(\mu) = L_2(\mu) = 0$ and ignore the loop-induced logarithmic corrections to the scattering amplitudes. The resulting amplitudes are universal in the sense that they depend only on v. They reproduce the low-energy theorems of pion dynamics. We unitarize these amplitudes by cutting off the partial waves when they saturate the bound $|a_\ell^I| < 1$. This is the original model considered by Chanowitz and Gaillard [2], so we call it *LET CG*.

2) For comparison, we consider another model in which we take $L_1(\mu) = L_2(\mu) = 0$ and ignore the loop-induced logarithmic corrections. This time, however, we unitarize the scattering amplitudes using a "K-matrix;" that is, we replace the partial wave amplitudes a_ℓ^I by t_ℓ^I, where

$$t_\ell^I = \frac{a_\ell^I}{1 - i a_\ell^I} . \tag{3.31}$$

We call this model *LET K*.

3) The third nonresonant model we consider includes the full $\mathcal{O}(p^4)$ amplitude presented above. By varying the parameters $L_1(\mu)$ and $L_2(\mu)$, one can sweep over all possible nonresonant physics. In particular, one can search for a region where unitarity violation is delayed up to 2 TeV. Scanning the $(L_1(\mu), L_2(\mu))$ parameter space, one finds that the values

$$\begin{aligned} L_1(\mu) &= -0.26 \\ L_2(\mu) &= +0.23 , \end{aligned} \tag{3.32}$$

measured at the renormalization scale $\mu = 1.5$ TeV, delay unitarity breakdown until 2 TeV. With these parameters, the amplitudes (3.30) are unitary, chiral and crossing-symmetric for energies up to 2 TeV. Beyond 2 TeV, the partial waves are no longer unitary. In order to compare with the total event rates in the other models, we unitarize the scattering amplitudes using the K-matrix prescription, so we call this model *DELAY K*. Note that only the real part of a_ℓ^I, from (3.13) and (3.30), is used to obtain the unitarized partial wave amplitude t_ℓ^I.

In what follows we use these models to represent new physics that is not resonant at SSC and LHC energies.

4. Numerical Results

We now turn to the background and signal results for the models discussed in sections 2 and 3. We begin by briefly summarizing our procedures and assumptions and then estimate the overall systematic error associated with the event rates to be presented.

In all our results, we use the leading-order parton distributions of Morfin and Tung [47], and include only the first four quark flavors as partons. In particular, we ignore the bottom quark as an initial-state parton. In computing signal event rates, we evaluate the parton distribution functions at the scale M_W. As discussed in Ref. 48, the agreement between the exact $W_L W_L$ production rates and those predicted by the effective–W approximation is best for this (natural) choice of scale. In a recent analysis that includes the next-order QCD corrections [49], it was found that for this choice of scale the QCD corrections to the WW scattering processes are very small, which indicates that the current tree-level calculations for the signals are rather reliable. The scales used in the background calculations depend upon the process, and are given in the references quoted in section 2. In general, the choices of scale are either strongly motivated on theoretical grounds or are those leading to the smallest higher–order corrections. To estimate the systematic error that is associated with our background rates because of scale choice and higher–order corrections, we need higher-order calculations which are not available at present. In the TeV region, however, the typical scales are large. This makes the strong coupling small and takes the parton distribution functions into regimes of relatively large momentum fraction, which are well-represented by experimental data.

To check the accuracy of employing the effective–W approximation in combination with the equivalence theorem (EWA/ET), we present a comparison in Table 4. For the test case of the Standard Model with a 1 TeV Higgs boson, the agreement between this approximate technique (EWA/ET) and the "subtraction" result using the full SM matrix element calculation (Subtraction) is reasonably good and generally becomes best at large invariant mass of the final state WW pair. However, in the W^+W^+ final state the agreement is excellent for all mass cuts examined. For other channels, the discrepancy at lower $M(WW)$ potentially derives from two sources: (a) use of the EWA for the longitudinally polarized W–boson scattering amplitudes, and (b) unavoidable inconsistencies associated with implementing the equivalence theorem, leading to a difference between EWA/ET and EWA/LL. (The EWA/LL approximation is that in which the EWA is employed in conjunction with the full longitudinal W–boson scattering amplitudes.) Regarding (a), we note that the derivation of the EWA intrinsically relies on $M(WW)$ being large. Thus, it is natural that some deviation between the Subtraction and EWA computations for the $W_L W_L$ final state could appear at low WW invariant mass. However, the close agreement between the exact and EWA/ET results for the W^+W^+ channel suggest that this source of deviation is quite small. This is because W^+W^+, being non-resonant, does not suffer from difficulties of type (b). Indeed, good agreement between exact and EWA/LL calculations for the (opposite charge)

Table 4: SM signal cross section comparison between the Subtraction results of Eq. (2.2) and the EWA/ET results (m_H =1 TeV) at the SSC, $\sqrt{s}$ = 40 TeV, in units of fb. Only the leptonic cuts in Table 1 are imposed.

ZZ	Subtraction	EWA/ET SM
$M_{ZZ} > 0.5$	1.0	1.9
$M_{ZZ} > 1.0$	0.52	0.69
$M_{ZZ} > 1.5$	0.06	0.08
W^+W^-	Subtraction	EWA/ET SM
$M_{\ell\ell} > 0.25$	9.0	12.6
$M_{\ell\ell} > 0.5$	7.8	12.1
$M_{\ell\ell} > 1.0$	0.68	1.0
W^+Z	Subtraction	EWA/ET SM
$M_T > 0.5$	0.29	0.33
$M_T > 1.0$	0.17	0.13
$M_T > 1.5$	0.08	0.05
W^+W^+	Subtraction	EWA/ET SM
$M_{\ell\ell} > 0.25$	0.90	0.93
$M_{\ell\ell} > 0.5$	0.47	0.46
$M_{\ell\ell} > 1.0$	0.10	0.10

W^+W^- channel has been found in earlier work [50] where the ET approximation was not employed. The main difference of type (b), *i.e.* between EWA/LL and EWA/ET, arises from our procedure of employing the Breit–Wigner prescription for s-channel resonances. As discussed below, if this procedure is employed (in the SM) for both a direct calculation of $W_LW_L \to W_LW_L$ using true W-boson fields and in the ET calculation of the same process, a large discrepancy is found for $M(WW)$ below the Higgs mass. The net deviation between the full matrix element calculation, as defined in Eq. (2.2), and the EWA/ET is displayed in Table 4.

Let us discuss briefly the inconsistencies associated with employing the Breit–Wigner prescription for the s-channel resonances in the scattering amplitudes. These were studied in the case of a heavy SM Higgs boson in Ref. 35. As already noted, the Breit–Wigner procedure for putting the width into the directly computed $W_LW_L \to W_LW_L$ amplitudes with true longitudinally polarized gauge bosons does not yield the same result as the identical procedure in the equivalence-theorem calculation. However, it is easily demonstrated that this violation of the equivalence theorem is higher–order in the perturbative expansion. When the width is small, the perturbative expansion is valid and the violation is tiny. For large

width, the Breit–Wigner procedure yields a significant violation of the equivalence theorem for $M(WW)$ below the resonance mass, but an unambiguous treatment is impossible because the perturbative expansion is breaking down. Our procedure can simply be viewed as defining a particular model for W_LW_L production. The second effect of adding the width through the Breit–Wigner prescription is to give a small violation of unitarity in the partial waves which contain the resonance. This can again be traced to a breakdown of the perturbative calculation and the Breit–Wigner induced violation of the equivalence theorem. This small violation of unitarity near the resonance can be safely ignored. Much more important is our demand that the unitarity conditions hold away from the resonance, in particular up to the highest $M(WW)$ scale of interest. Indeed, our cuts automatically emphasize the large $M(WW)$ region in which the Breit–Wigner procedure becomes immaterial. Thus, as already stated, we see no reason to anticipate large errors in our signal rates in the large $M(WW)$ region.

Finally, we remind the reader that our *signal* is defined as the number of W_LW_L pairs produced in any given channel. In general, this is not the same as one would obtain by plotting events as a function of $M(WW)$ and then subtracting a smooth background under some "bump" in the distribution. Even in the fully reconstructable four-lepton final state of the ZZ channel, a spin–zero isospin–zero resonance is significantly above the continuum background at high $M(ZZ)$, well beyond the obvious bump in the distribution. Indeed, in non-resonant channels, such as W^+W^+, there is no visible bump in $M(WW)$. And, for most of the final states considered, the missing neutrinos make full reconstruction of the WW mass impossible in any case. The ability to detect the signal will thus ultimately depend upon the accuracy with which the expected rate for WW production in the LT and TT polarization modes can be computed. As we have already emphasized, the SM computation (with a light Higgs boson) gives an accurate result for this rate.

The signal and background rates that we shall quote are only as good as the parton distributions and parton-level Monte Carlo programs employed. Significant improvements in both will be made once data from HERA is available. Also, the required parton distributions will be determined to high accuracy by other high-p_T and Drell-Yan pair measurements at the SSC or LHC, and implementation of the cuts by each detector collaboration will become very well understood as experience with the apparatus accumulates and the full hadronic-level Monte Carlo simulations are fine-tuned at SSC/LHC energies. In particular, the background levels in the various channels should become sufficiently well-determined that any significant LL (*i.e.* W_LW_L) excess will be evident. Although at present we are confined to parton-level predictions, our results should give a reliable indication of the ultimate rates for the background and signal that can be achieved in each model after appropriate cuts.

We summarize our results in Tables 5a and 5b for the SSC and the LHC, respectively. These tables give the event rates for the summed background and for the signal in each of the models as a function of the mass cut placed on the final state. The particular type of

Table 5a: Event rates per SSC-year, assuming $m_t = 140$ GeV, $\sqrt{s} = 40$ TeV, and an annual luminosity of 10 fb^{-1}. Cuts are listed in Table 1.

ZZ	Bkgd.	SM	Scalar	$O(2N)$	Vec 2.0	Vec 2.5	LET CG	LET K	Delay K
$M_{ZZ} > 0.5$	1.0	11	6.2	5.2	1.1	1.5	2.6	2.2	1.6
$M_{ZZ} > 1.0$	0.3	4.1	2.6	2.0	0.4	0.7	1.6	1.3	0.8
$M_{ZZ} > 1.5$	0.1	0.5	0.2	0.5	0.1	0.3	0.9	0.6	0.4
W^+W^-	Bkgd.	SM	Scalar	$O(2N)$	Vec 2.0	Vec 2.5	LET CG	LET K	Delay K
$M_{\ell\ell} > 0.25$	21	48	30	24	15	12	16	12	11
$M_{\ell\ell} > 0.5$	17	46	29	23	15	12	15	11	11
$M_{\ell\ell} > 1.0$	3.6	3.8	1.1	2.7	6.5	4.9	5.3	3.6	4.6
W^+Z	Bkgd.	SM	Scalar	$O(2N)$	Vec 2.0	Vec 2.5	LET CG	LET K	Delay K
$M_T > 0.5$	2.5	1.3	1.8	1.5	9.5	6.2	5.8	4.9	6.0
$M_T > 1.0$	0.8	0.5	0.8	0.7	7.9	4.7	4.1	3.3	4.6
$M_T > 1.5$	0.3	0.2	0.2	0.3	5.5	3.2	2.6	1.9	3.2
W^+W^+	Bkgd.	SM	Scalar	$O(2N)$	Vec 2.0	Vec 2.5	LET CG	LET K	Delay K
$M_{\ell\ell} > 0.25$	3.5	6.4	8.2	7.1	7.8	11	25	21	15
$M_{\ell\ell} > 0.5$	1.5	3.2	4.2	3.9	3.8	6.3	19	15	11
$M_{\ell\ell} > 1.0$	0.2	0.7	0.6	0.9	0.5	1.2	7.6	5.2	5.2

mass cut is channel dependent, and has been detailed in section 2. For each channel, the second mass cut for which we tabulate results is the minimum for which we deem the the EWA/ET approximation to be reliable for all the different models. For instance, in the case of the SM, Scalar and $O(2N)$ models, the optimal cut on $M(\ell\ell)$ in the W^+W^- channel is of order 500 GeV. For such a cut, contributing $M(WW)$ values are large enough that the EWA/ET approximation is quite good. Results for other cuts illustrate how rapidly the event levels fall off with increasing invariant mass cut. Lower cuts might be reliable for some channels in the case of some models. For instance, in the W^+W^- channel, the LET CG, LET K, and Delay K models all lack resonance structure of any kind, and the EWA/ET approximation might be adequate for $M(\ell\ell) \gtrsim 250$ GeV. In Fig.3 we show distributions in the mass variables for several different models at the SSC. Of course, the number of events expected (see the tables) is generally much too small to allow for an actual measurement of these mass distributions. However, the distributions allow for some intuitive feeling as to where the signal event rates are largest and how rapidly the rates decline with increasing invariant mass.

From the tables it is apparent that the absolute number of (leptonic channel) signal events in one SSC 10 fb^{-1} year or one LHC 100 fb^{-1} year is never large. However, our cuts

Table 5b: Event rates per LHC-year, assuming $m_t = 140$ GeV, $\sqrt{s} = 16$ TeV, and an annual luminosity of 100 fb^{-1}. Cuts are listed in Table 1.

ZZ	Bkgd.	SM	Scalar	$O(2N)$	Vec 2.0	Vec 2.5	LET CG	LET K	Delay K
$M_{ZZ} > 0.5$	1.0	14	7.5	6.4	1.4	1.7	2.5	2.2	1.8
$M_{ZZ} > 1.0$	0.1	3.9	2.7	1.8	0.4	0.6	1.1	0.9	0.6
$M_{ZZ} > 1.5$	0.0	0.3	0.1	0.3	0.1	0.2	0.4	0.3	0.2
W^+W^-	Bkgd.	SM	Scalar	$O(2N)$	Vec 2.0	Vec 2.5	LET CG	LET K	Delay K
$M_{\ell\ell} > 0.25$	18	40	26	19	8.0	6.8	9.2	7.2	6.2
$M_{\ell\ell} > 0.5$	15	32	21	16	7.4	6.1	8.3	6.3	5.5
$M_{\ell\ell} > 1.0$	2.5	1.3	0.4	1.0	2.4	1.6	1.7	1.1	1.2
W^+Z	Bkgd.	SM	Scalar	$O(2N)$	Vec 2.0	Vec 2.5	LET CG	LET K	Delay K
$M_T > 0.5$	2.4	1.0	1.4	1.1	4.8	3.2	3.2	2.9	3.0
$M_T > 1.0$	0.3	0.3	0.4	0.3	3.3	1.8	1.6	1.4	1.7
$M_T > 1.5$	0.1	0.1	0.1	0.1	2.0	1.0	0.8	0.6	0.9
W^+W^+	Bkgd.	SM	Scalar	$O(2N)$	Vec 2.0	Vec 2.5	LET CG	LET K	Delay K
$M_{\ell\ell} > 0.25$	6.2	9.6	12	10	12	16	27	24	16
$M_{\ell\ell} > 0.5$	1.7	3.7	5.2	4.3	4.8	7.3	16	14	8.3
$M_{\ell\ell} > 1.0$	0.2	0.4	0.5	0.6	0.4	1.0	4.2	2.9	2.3

have reduced backgrounds to a remarkably low level, so that even a relatively small number of excess LL events should be observable. Consequently, we find that for each model, whether it has a scalar resonance, a vector resonance, or no resonance at all, there is always a WW charged-lepton mode for which the signal is larger than background. For instance, for the SM, the Scalar resonance model and the $O(2N)$ model, the electroweak symmetry sector contains a spin–zero isospin–zero resonance. As a result, the signal rates in the ZZ and W^+W^- channels are clearly above the background. Similarly, the signal event rate in the W^+Z mode is larger than the background rate for the two Vector models with a spin–one isospin–one resonance. Finally, the W^+W^+ mode has the most significant event rate in the LET CG, LET K, and Delay K models that have no resonance.

To quantify the observability of a given signal above background, we proceed as follows. We define the signal to be observable at a confidence level of $P\%$ if the maximum number of background events, B_{max} at $P\%$ confidence level is smaller than the minimum number of signal *plus* background events, SB_{min}, at $P\%$ confidence level. Here, B_{max} is the number of background events such that the probability of having any number up to and including B_{max} is $0.01\,P$, while SB_{min} is the number of signal plus background events such that the probability of having a number greater than or equal to SB_{min} is $0.01\,P$. For a 99%

confidence level signal, these two probabilities are 0.99. The values B_{max} and SB_{min} are computed assuming Poisson statistics. For integer values, this means that we require

$$0.01\,P = \sum_{n=0}^{B_{max}} \frac{B^n}{n!} e^{-B}; \quad 0.01\,P = \sum_{n=SB_{min}}^{\infty} \frac{(S+B)^n}{n!} e^{-(S+B)}, \tag{4.1}$$

where B and $S+B$ are the background and signal plus background rates, respectively.* B and S are obtained as a function of luminosity from the event rates tabulated earlier for the different types of models by scaling with respect to the luminosities of 10 fb^{-1} and 100 fb^{-1} adopted for the SSC and LHC, respectively, in constructing the tables. We will uniformly employ results for the middle (second) mass cut tabulated for each channel. Even though backgrounds decrease rapidly with increasing invariant mass cut, the signal also decreases (though less rapidly) and the limited resulting statistics are such that there is no channel for which the higher (third) mass cut tabulated in Tables 5a and 5b leads to a more observable signal at either the 99% or 95% confidence level.

As an example, consider again the W^+W^- channel and the SM, Scalar and $O(2N)$ models (for integrated luminosity of 10 fb^{-1} at the SSC). For all three models, the background rate of 17 events is smaller than the signal rates. The smallest signal rate among the three models for the $M_{\ell\ell} \geq 0.5$ TeV cut is the 23 events predicted for the $O(2N)$ model. The 99% confidence level upper limit on the background is 27 events, whereas for the $O(2N)$ model the 99% confidence level lower limit on signal plus background is 25 events. Thus, the predicted signal is not quite observable at the 99% confidence level for the $O(2N)$ model. In contrast, 99% confidence level *is* achieved for the SM and Scalar models in the W^+W^- channel after (less than) one 10 fb^{-1} year.

The simplest manner in which the observability of all the various signals can be tabulated is to give the number of years required to achieve a signal at a given confidence level for each channel and each model. (Of course, if the machine can be run at a higher instantaneous luminosity the required integrated luminosities can be achieved in less than the time indicated.) These results for the SSC and LHC appear in Tables 6 and 7, respectively. Let us first discuss the SSC results. In Table 6a (6b) we give the number of 10 fb^{-1} years required to see a signal in a given channel for a given model at a 99% (95%) confidence level, as defined above. As indicated earlier, the clearest signals for the SM, Scalar and $O(2N)$ models are obtained in the W^+W^- channel. The Vector models are most easily probed in the W^+Z channel. (Note, however, that for the Vector 2.5 model, the W^+W^+ channel is actually superior after imposing the kinematic cuts listed in Table 1.) Finally, the LET CG, LET K, and Delay K models are only readily probed using the W^+W^+ channel. This is not

* If the equalities in Eq. (4.1) are not satisfied for integer values of B_{max} and SB_{min}, we determine B_{max} and/or SB_{min} by interpolating between the two integer values such that the appropriate sum is just below and just above $0.01\,P$.

Table 6a: Number of years (if < 10) at SSC required for a 99% confidence level signal.

Channel\Model	SM	Scalar	$O(2N)$	Vec. 2.0	Vec. 2.5	LET CG	LET K	Delay K
ZZ	2.2	4.0	5.8			7.8		
W^+W^-	0.50	1.0	1.2	2.5	3.5	2.5	4.0	4.0
W^+Z				1.5	2.8	3.2	4.2	2.8
W^+W^+	6.2	4.0	4.5	4.8	2.2	0.50	0.75	1.2

Table 6b: Number of years (if < 10) at SSC required for a 95% confidence level signal.

Channel\Model	SM	Scalar	$O(2N)$	Vec. 2.0	Vec. 2.5	LET CG	LET K	Delay K
ZZ	1.2	2.2	3.0			4.0	5.5	
W^+W^-	0.25	0.50	0.75	1.2	1.8	1.2	2.0	2.0
W^+Z				0.75	1.5	1.8	2.2	1.5
W^+W^+	3.2	2.2	2.2	2.5	1.2	0.25	0.50	0.50

Table 7a: Number of years (if < 10) at LHC required for a 99% confidence level signal.

Channel\Model	SM	Scalar	$O(2N)$	Vec. 2.0	Vec. 2.5	LET CG	LET K	Delay K
ZZ	2.0	3.0	4.8			9.0		
W^+W^-	0.75	1.2	2.0	7.5		6.0		
W^+Z				3.0	6.8	7.8	9.5	7.2
W^+W^+	5.2	3.2	4.2	3.5	2.0	0.75	0.75	1.8

Table 7b: Number of years (if < 10) at LHC required for a 95% confidence level signal.

Channel\Model	SM	Scalar	$O(2N)$	Vec. 2.0	Vec. 2.5	LET CG	LET K	Delay K
ZZ	1.2	1.8	2.5			4.8	6.0	
W^+W^-	0.50	0.75	1.0	3.8	5.2	3.0	5.0	6.5
W^+Z				1.8	3.5	4.0	4.8	3.8
W^+W^+	2.8	1.8	2.2	2.0	1.0	0.50	0.50	1.0

to say that other channels are useless, especially if a 95% confidence level signal is deemed adequate. Relatively small numbers of years (< 2.5) are required to observe a signal at 95%

Table 8: Percentage decrease in the SSC event rate for the W^+W^- channel relative to the $\cos\phi_{\ell\ell} < -0.8$ cut results presented in Table 5a.

W^+W^-	Bkgd.	SM	Scalar	$O(2N)$	Vec 2.0	Vec 2.5	LET CG	LET K	Delay K
$\cos\phi_{\ell\ell} < -0.96$	25	3.7	4.3	3.5	2.3	2.3	2.0	2.2	2.2

confidence level in all cases except: the W^+Z channel for the SM, Scalar and $O(2N)$ models; the ZZ channel for the $O(2N)$, Vector, and LET/Delay models; and the W^+W^+ channel for the SM.

Of course, in the case of the W^+W^+ and W^+Z channels we may also add in the opposite sign modes. Because of the fact that the down-quark distribution function is smaller than that for the up quark at moderate-to-large x (high invariant masses probe fairly sizeable x values), these event rates are always smaller than those of the positive charge channels. One finds that the W^-W^- signal event rate is about $1/3 \sim 1/2$ of the W^+W^+ rate. Similarly, the ratio of W^-Z to W^+Z signal event rates is about $1/2 \sim 2/3$ for the models considered here. Meanwhile, the irreducible $TT + LT$ background rates decrease by about a factor of $2/3$ in both channels. By combining the channels of both charge, the observability of the $W^+W^+ + W^-W^-$ and $W^+Z + W^-Z$ signals is somewhat enhanced over the results given in the tables. It is important to note that one of the best means for checking that we are observing the signal of interest is to measure the ratio of W^+W^+ to W^-W^- and W^+Z to W^-Z, respectively. Should the ability of the detectors to discriminate between lepton charges at high momentum be inadequate, we would expect these ratios to be near unity.

In obtaining our LHC results, we have used cuts (as detailed in section 2) that are closely analogous to those employed for the SSC. In so doing, we did not attempt to optimize the cuts to the same extent as we did for the SSC. Thus, it is possible that the signal/background ratios could be improved, although we do not anticipate that further optimization would lead to any dramatic changes. From Tables 7a and 7b we see that in the W^+Z, ZZ and W^+W^+ channels the LHC with a 100 fb^{-1} luminosity is roughly equivalent to the SSC with 10fb^{-1}, except for the Vector models. Because of the large resonance masses, the Vector models are much more difficult to see at the LHC than at the SSC. In the W^+W^- channel, the SSC has a distinct advantage over the LHC for all models. This is due to the relatively greater difficulty in removing the $t\bar{t}$ background at the LHC. Another issue of concern for the LHC is the large probability of having multiple interactions in one crossing, yielding many minimum-bias and mini-jet events superimposed on each WW event of interest. This type of pileup is likely to significantly increase the background levels beyond those computed here on the basis of one collision per crossing. In addition, isolation criteria, the central jet-veto, and jet-tagging, all of which are central to our analysis, could become much more difficult to implement. In this case, detection of strong interactions in the various W_LW_L channels

would be substantially more difficult at the LHC than at the SSC.

5. Discussion

An important question is the extent to which we have truly optimized the procedures for isolating an LL signal in the various WW purely-leptonic final state channels. Below we discuss several improvements that might turn out to be feasible.

A possible improvement in the significance of the signals in the W^+W^- and W^+W^+ channels can be obtained by tightening the cut on $\cos\phi_{\ell\ell}$. The improvement that can be obtained, based on our EWA/ET parton-level Monte Carlo, is illustrated in Table 8 in the case of the W^+W^- channel. By tightening the cut from $\cos\phi_{\ell\ell} < -0.8$ to $\cos\phi_{\ell\ell} < -0.96$, the background is reduced to 3/4 of its previous size while the LL signal rate is decreased by at most 4% (in the SM and Scalar cases) and perhaps, by as little as 2% (Vector and LET CG models). Such a large decrease in the background level would clearly lead to an increase in the significance of the signals in these channels.

However, these results were obtained using the EWA/ET calculation in which the transverse momentum of the W_LW_L pair, $p_T(WW)$, is ignored. A non-zero value for $p_T(WW)$ would imply that the W_LW_L are not exactly back-to-back. Previously, we noted the $1/(p_T^2 + M_W^2)^2$ distribution of the W_L's which initiate the W_LW_L scattering (as measured with respect to the quarks from which they are emitted). This steep fall-off implies that $p_T(WW)$ for the W_LW_L signal is very limited (in contrast to the W_LW_T and W_TW_T background). Typically, $p_T(WW)$ for the W_LW_L scattering signal is not much larger than M_W. For an event with $p_T(W) \sim 0.5$ TeV, $p_T(WW) \sim M_W$ can result in angle of $\phi \approx 162^\circ$ (for the configuration where $p_T(WW)$ is perpendicular to the individual p_T's of the W's), which corresponds to $\cos\phi(WW) \approx -0.95$. Thus, although the agreement between the exact "subtraction" calculation and the EWA/ET calculation is excellent for a modest cut at -0.8, as illustrated by the W^+W^+ comparison of Table 4, this agreement might worsen if the cut is strengthened. Indeed, in the W^+W^- channel we have found that the exact "subtraction" result with $\cos\phi_{\ell\ell} < -0.96$ is about 23% as much as that with $\cos\phi_{\ell\ell} < -0.8$, as compared to the 4% decrease listed in Table 8 obtained using the EWA/ET amplitudes. Further, there are additional sources of $p_T(WW)$. A Monte Carlo which goes beyond the parton level will include initial-state radiation of gluons, the intrinsic transverse momentum of the quarks that initially radiate the fusing W's, and hard gluon radiation in the final state (part of the higher-order QCD corrections to the W_LW_L scattering process). All of these effects will tend to impart some net transverse momentum to the W_LW_L pair and decrease the fraction of lepton pairs that are sufficiently back-to-back to pass a very severe cut on $\cos\phi_{\ell\ell}$. We anticipate that the -0.8 cut is sufficiently moderate that such effects will not significantly alter the efficiencies obtained from a parton Monte Carlo. It is worthwhile to notice that the effects of $p_T(WW)$ are less important for models with more events in the larger mass

region ($M(WW) > 1$ TeV), such as LET CG. This was also demonstrated in Ref. 31. where an empirical formula for the $p_T(WW)$ spectrum was used in combination with the EWA.

Regardless of which $\cos\phi_{\ell\ell}$ cut turns out to be most appropriate, one can ask whether it would be beneficial in the ZZ and WZ channels. We have not imposed this cut in our work because background event rates in these channels are already small after the cuts employed, and the amount of improvement in the significance of a signal would be marginal. It is only if some of the cuts that we *have* employed must be significantly weakened, or if our cuts are not so efficient in eliminating the background, when the actual data is analyzed, that a $\cos\phi_{\ell\ell}$ cut in these channels might prove valuable.

Another issue is the extent to which our cuts eliminate a contribution to the LL signals of interest arising from a source quite distinct from the W_LW_L scattering processes upon which we have focused. An example of such a situation arises in the case of the WZ channel. If the appropriate model contains a spin–one isospin–one resonance, then a larger signal rate is obtained by eliminating the jet-tag cut. This is because there is an additional contribution from $q\bar{q}$ fusion in which a virtual W is created that then mixes with the vector resonance. Some analysis of this situation has appeared in Refs. [42,51,52], where it was found that one might be able to observe a signal without jet-tagging if such a resonance exists. However, eliminating the jet-tagging is much more likely to be viable at the SSC than at the LHC. In Tables 2a and 2b, we saw that the signal/background ratio becomes much worse at the LHC than at the SSC if jet-tagging is not performed. Clearly, a careful study is required; this is beyond the scope of the present paper.

We must not forget that, for each channel, we have considered only the "gold–plated" purely-leptonic decay modes containing the maximum possible number of charged leptons. These are the cleanest modes for observing the LL signal, but a significant price is paid in terms of branching ratios. The next-most clean mode that can be considered is $ZZ \to \ell^+\ell^-\nu\bar{\nu}$. This mode has roughly six times as large a branching ratio as the four-charged-lepton mode we have studied. Parton-level calculations [53] and some recent SDC detector studies [29] indicate that cuts can be implemented which could eliminate reducible backgrounds in this mode. The only issue is the extent to which the irreducible EW $Z_TZ_T + Z_TZ_L$ backgrounds can be suppressed. Some study of this has appeared in Ref. 51. There, it is found that a significant improvement in the observability of the Z_LZ_L signal can be obtained for several models if the $\ell^+\ell^-\nu\bar{\nu}$ mode is employed.

Of course, WW final states containing a mixture of leptons and jets have still higher branching ratios. However, mixed QCD-electroweak backgrounds enter. Many of the techniques that we have developed here for isolating the purely leptonic signals will also be applicable for such mixed states, and additional cuts will become relevant, *e.g.* a cut on multiplicity and/or rapidity structure [54,55]. A refined study of the mixed modes, incorporating some of the procedures that have been developed for the purely leptonic modes, should be performed [6], but is beyond the scope of this paper.

We have demonstrated the importance of using the single jet-tagging to enhance the signal/background ratio, especially for the W^+W^- mode to suppress the huge $t\bar{t}$ background [14]. Our resulting tagging efficiency for the signal agrees well with the full Monte Carlo study for the SDC detector [29]. This is also true for the background process $t\bar{t}j$;* our fixed order α_s^3 parton-level calculation agrees quite well with results quoted in the SDC report [29]. Nonetheless, still more careful studies of jet-tagging in the forward/backward region would be worthwhile.

6. Conclusions

We have demonstrated that, at both the SSC and the LHC, viable signals for strong W_LW_L interactions can be obtained for a wide variety of models in the purely leptonic final states. Of course, the channels examined, $W^+W^- \to \ell^+\ell^-\nu\bar{\nu}$, $W^+Z \to \ell^+\ell^-\ell\nu$, $ZZ \to \ell^+\ell^-\ell^+\ell^-$, and $W^+W^+ \to \ell^+\ell^+\nu\nu$, do not *all* yield adequate signals in 1-2 years of canonical SSC or LHC luminosity for *all* models. Instead, we find that a significant signal can always be found in the channels that most naturally complement the particular type of model considered. In particular, models with a resonance of definite isospin are most easily probed using the WW channels that have resonant contributions from that same isospin. Indeed, one of our more important conclusions is that different types of models can be distinguished experimentally by determining the relative magnitude of the LL signals in the four channels listed above.

A large part of our work focused on the techniques required to suppress reducible and, especially, irreducible backgrounds to a level such that the low LL signal event rates in the purely leptonic channels can be isolated. In particular, the irreducible backgrounds from production of WW pairs with TT and LT polarizations end up being most important, and our techniques are particularly focused on suppressing them. Although our calculations do not include detector effects, we believe that they will survive more sophisticated Monte Carlo analyses. In particular, the types of cuts we have employed should be directly applicable in the experimental analyses that will be performed when actual data becomes available.

Overall, we conclude that it is possible to probe a strongly interacting electroweak symmetry breaking sector at the SSC or LHC using only the "gold-plated" purely-leptonic modes studied here. Even if a light Higgs boson is found, it will be important to measure the event rates at high $M(WW)$ in all the various channels in order to make certain that the Higgs boson completely cures the bad high-energy behavior in all WW scattering subprocesses. The low event rates for the purely-leptonic final states imply that of order 2-3 years of 10 fb^{-1} annual luminosity will be required to conclude that there is no obvious W_LW_L enhancement

* In preliminary versions of this work, a programming error led to an apparent disagreement [14].

in any of the four channels. Because of the relative cleanliness of these final states, the option of achieving this required integrated luminosity via enhanced instantaneous luminosity should be strongly considered.

Acknowledgements: We would like to thank M. Berger, M. Chanowitz, S. Dawson, K. Hikasa, G. Kane, S. Mrenna, S. Naculich, J. Ohnemus, L. Orr, F. Paige, R. Phillips, C. Quigg, W. Repko, R. Stuart, G. Valencia, E. Wang, S. Willenbrock, H. Yamamoto, and D. Zeppenfeld for many helpful discussions. The work of J. Bagger was supported in part by NSF grant PHY-9096198 and in part by Texas National Research Laboratory Commission (TNRLC) grant RGFY93292. The work of V. Barger was supported in part by DOE grant DE-AC02-76ER00881 and in part by TNRLC grant RGFY9273. The work of K. Cheung was supported in part by DOE grant DE-FG02-91-ER40684. The work of J. Gunion was supported in part by DOE grant DE-FG-03-91ER40674. T. Han was supported in part by TNRLC Awards No. FCFY9116. The work of G. Ladinsky was supported in part by DOE grant DE-FG02-90ER-40577 and TNRLC grant RGFY9240. The work of R. Rosenfeld and C.-P. Yuan was supported in part by TNRLC grant RGFY9114 and RGFY9240, respectively.

REFERENCES

1. D. A. Dicus and V. S. Mathur, Phys. Rev. **D7**, 3111 (1973); B. W. Lee, C. Quigg, and H. Thacker, Phys. Rev. **D16**, 1519 (1977); M. Veltman, Acta Phys. Polon. **B8**, 475 (1977).
2. M. S. Chanowitz and M. K. Gaillard, Nucl. Phys. **B261**, 379 (1985).
3. J. M. Cornwall, D. N. Levin, and G. Tiktopoulos, Phys. Rev. **D10**, 1145 (1974); C. Vayonakis, Lett. Nuovo Cimento **17**, 383 (1976); G. J. Gounaris, R. Kogerler, and H. Neufeld, Phys. Rev. **D34**, 3257 (1986); Y.-P. Yao and C.-P. Yuan, Phys. Rev. **D38**, 2237 (1988); J. Bagger and C. R. Schmidt, Phys. Rev. **D41**, 264 (1990); H. Veltman, Phys. Rev. **D41**, 2294 (1990); H.-J. He, Y.-P. Kuang and Xiaoyuan Li, Phys. Rev. Lett. **69**, 2619 (1992).
4. M. S. Chanowitz and M. K. Gaillard, Phys. Lett. **B142**, 85 (1984); G. L. Kane, W. W. Repko and W. R. Rolnick, Phys. Lett. **B148**, 367 (1984); S. Dawson, Nucl. Phys. **B249**, 42 (1985).
5. J. Lindfors, Z. Phys. **C28**, 427 (1985); J. F. Gunion, J. Kalinowksi, and A. Tofighi-Niaki, *Phys. Rev. Lett.* **57**, 2351 (1986); W. B. Rolnick, Nucl. Phys. **B274**, 171 (1986); P. W. Johnson, F. I. Olness and Wu-Ki Tung, Phys. Rev. **D36**, 291 (1987); Z. Kunszt and D. E. Soper, Nucl. Phys. **B296**, 253 (1988); A. Abbasabadi, W. W. Repko, D. A. Dicus and R. Vega, Phys. Rev. **D38**, 2770 (1988); S. Dawson, Phys. Lett. **B217**, 347 (1989).
6. For a review, see C.-P. Yuan, *Proposal for Studying TeV $W_LW_L \to W_LW_L$ Interactions Experimentally*, preprint MSUTH 92/06, 1992, to be published in *Perspectives On Higgs Physics*, edited by Gordon L. Kane, World Scientific Publishing Company, in press.
7. J. Kuti, L. Lin, and Y. Shen, Phys. Rev. Lett. **61**, 678 (1988); M. Luscher and P. Weisz, Phys. Lett. **B212**, 472 (1988); Nucl. Phys. **B318**, 705 (1989); U. M. Heller *et al.*, FSU-SCRI-93-29 (1993).
8. J. F. Gunion *et al.*, Ref. 5.
9. R. N. Cahn *et al.*, Phys. Rev. **D35**, 1626 (1987); V. Barger, T. Han, and R. J. N. Phillips, Phys. Rev. **D37** 2005 (1988); R. Kleiss and W. J. Stirling, Phys. Lett. **200B**, 193 (1988).
10. D. Froideveaux, Proceedings of the LHC Workshop (1990), CERN 90-10, Vol II, p. 444; M. H. Seymour, *ibid.* p. 557.
11. U. Baur and E. W. N. Glover, Nucl. Phys. **B347**, 12 (1990); U. Baur and E. W. N. Glover, Phys. Lett. **B252**, 683 (1990).
12. V. Barger, K. Cheung, T. Han, and R.J.N. Phillips, Phys. Rev. **D42**, 3052 (1990).

13. V. Barger, K. Cheung, T. Han, J. Ohnemus, and D. Zeppenfeld, Phys. Rev. **D44**, 1426 (1991).

14. V. Barger, K. Cheung, T. Han, and D. Zeppenfeld, Phys. Rev. **D44**, 2701 (1991); Erratum to appear in Phys. Rev. D; MAD/PH/757.

15. V. Barger, K. Cheung, T. Han, A. Stange, and D. Zeppenfeld, Phys. Rev. **D46**, 2028 (1992).

16. D. Dicus, J.F. Gunion, and R. Vega, Phys. Lett. **258B**, 475 (1991).

17. D. Dicus, J.F. Gunion, L. H. Orr, and R. Vega, Nucl. Phys. **B377**, 31 (1991).

18. talks given by W. Smith, F. Paige, and T. Han at the *SSC Physics Symposium*, Madison, Wisconsin, Feb. 1991 (unpublished).

19. R. W. Brown and K. O. Mikaelian, Phys. Rev. **D19**, 922 (1979).

20. U. Baur, E. W. N. Glover, and J. J. van der Bij, Nucl. Phys. **B318**, 106 (1989); V. Barger, T. Han, J. Ohnemus, and D. Zeppenfeld, Phys. Rev. **D41**, 2782 (1990).

21. J. Ohnemus and J. F. Owens, Phys. Rev. **D43**, 3626 (1991); B. Mele, P. Nason, and G. Ridolfi, Nucl. Phys. **B357**, 409 (1991).

22. D. A. Dicus, C. Kao, and W. W. Repko, Phys. Rev. **D36**, 1570 (1987); E. W. N. Glover and J. J. van der Bij, Nucl. Phys. **B321**, 561 (1989).

23. D. A. Dicus, S. L. Wilson, and R. Vega, Phys. Lett. **192B**, 231 (1987).

24. V. Barger, T. Han, and R. J. N. Phillips, Phys. Lett. **200B**, 193 (1988); U. Baur and E. W. N. Glover, Phys. Rev. **D44**, 99 (1991).

25. R. K. Ellis and J. C. Sexton, Nucl. Phys. **B282**, 642 (1987).

26. P. Nason, S. Dawson, and R. K. Ellis, Nucl. Phys. **B303**, 607 (1988); W. Beenakker *et al.*, Phys. Rev. **D40**, 54 (1989); Nucl. Phys. **B351**, 507 (1991).

27. R. Kleiss and W. J. Stirling, Z. Phys. **C40**, 419 (1988); H. Baer, V. Barger, and R. J. N. Phillips, Phys. Rev. **D39**, 2809 (1989); H. Baer, V. Barger, J. Ohnemus, and R. J. N. Phillips, Phys. Rev. **D42**, 54 (1990); R. P. Kauffman and C.P. Yuan, Phys. Rev. **D42**, 956 (1990); G. A. Ladinsky and C.P. Yuan, Phys. Rev. **D43**, 789 (1990).

28. V. Barger, A. D. Martin, and R. J. N. Phillips, Phys. Lett. **B125**, 339(1983); V. Barger, T. Han, and J. Ohnemus, Phys. Rev. **D37**, 1174(1988).

29. SDC Technical Design Report, SDC-92-201 (1992).

30. M. S. Chanowitz and M. Golden, Phys. Rev. Lett. **61**, 1053 (1988); **63**, 466(E) (1989).

31. M. S. Berger and M. S. Chanowitz, Phys. Lett. **B263**, 509 (1991).

32. D. A. Dicus and R. Vega, Phys. Lett. **B217**, 194 (1989).

33. For a review, see *e. g.* , J. Bagger, in R. K. Ellis, C. T. Hill, and J. D. Lykken, eds., *Perspectives in the Standard Model*, World Scientific, 1992.

34. C.-P. Yuan, Nucl. Phys. **B310** (1988) 1.

35. G.L. Kane and C.-P. Yuan, Phys. Rev. **D40**, 2231 (1989).

36. S. Willenbrock and G. Valencia, Phys. Lett. **B247**, 341 (1990); Phys. Rev. **D46**, 2247 (1992).

37. M. Einhorn, Nucl. Phys. **B246**, 75 (1984).

38. S. Nachulich and C.-P. Yuan, Phys. Lett. **B293**, 395 (1992).

39. S. Weinberg, Phys. Rev. **166**, 1568 (1968); S. Coleman, J. Wess and B. Zumino, Phys. Rev. **177**, 2239 (1969); C. Callan, S. Coleman, J. Wess and B. Zumino, Phys. Rev. **177**, 2247 (1969); S. Weinberg, Physica **96A**, 327 (1979).

40. S. Weinberg, Phys. Rev. Lett. **17**, 616 (1966); M. S. Chanowitz, M. Golden, and H. Georgi, Phys. Rev. Lett. **57**, 2344 (1986); Phys. Rev. **D35**, 1490 (1987).

41. R. Casalbuoni, *et al.*, Phys. Lett. **B155**, 59 (1985); Nucl. Phys. **B282**, 235 (1987); see also M. Bando, T. Kugo, and K. Yamawaki, Phys. Rep. **164**, 217 (1988), and references therein.

42. R. Casalbuoni, *et al.*, Phys. Lett. **B249**, 130 (1990); **B253**, 275 (1991); J. Bagger, T. Han and R. Rosenfeld, in E. Berger, ed., *Research Directions for the Decade, Snowmass 1990,* World Scientific, 1992.

43. R. Casalbuoni, *et al.*, Phys. Lett. **B269**, 361 (1991).

44. A. Dobado, M. Herrero and J. Terron, Z. Phys. **C50**, 205 (1991); 465 (1991); S. Dawson and G. Valencia, Nucl. Phys. **B348**, 23 (1991); Nucl. Phys. **B352**, 27 (1991); J. Bagger, S. Dawson and G. Valencia, in E. Berger, ed., *Research Directions for the Decade, Snowmass 1990,* World Scientific, 1992.

45. J. Gasser and H. Leutwyler, Ann. Phys. **158**, 142 (1984); Nucl. Phys. **B250**, 465 (1985); J. Bagger, S. Dawson and G. Valencia, Fermilab preprint PUB-92-75-T (1992), and references therein.

46. See, however, A.F. Falk, M. Luke and E.H. Simmons, Nucl. Phys. **B365** (1991) 523.

47. J. G. Morfin and W.-K. Tung, Z. Phys. **C52**, 13 (1991).

48. M. Berger and M. Chanowitz, Phys. Lett. **B267**, 416 (1991).

49. T. Han, G. Valencia, and S. Willenbrock, Phys. Rev. Lett. **69**, 3274 (1992).

50. J. F. Gunion, J. Kalinowski, A. Tofighi-Niaki, A. Abbasabadi, and W. Repko, in *Physics of the Superconducting Supercollider*, Snowmass, Colorado (1986); Gunion *et al.*, Ref. 5; Abbasabadi *et al.*, Ref. 5.

51. M. Chanowitz, talk presented in the XXVI International Conf. on High Energy Physics, Dallas, Aug., 1992; and talk presented in the Workshop on Electroweak Symmetry Breaking at Colliding-Beam Facilities, University of California at Santa Cruz, December, 1992.

52. A. Dobado, M. J. Herrero, and T. N. Truong, Phys. Lett. **235**, 129 (1990).

53. R. N. Cahn and M. Chanowitz, Phys. Rev. Lett. **56**, 1327 (1986); V. Barger, T. Han, and R. Phillips, Phys. Rev. **D36**, 295 (1987).

54. J.F. Gunion *et al.*, Phys. Rev. **D40**, 2223 (1989).

55. J. D. Bjorken, Phys. Rev. **D47**, 101 (1993); SLAC-PUB-5823, talk given at the IXth International Workshop on Photon-Photon Collisions, University of California, San Diego, La Jolla, CA, March 23-27, 1992.

FIGURE CAPTIONS

1) Symbolic diagrams for the $W_LW_L \to W_LW_L$ scattering signal. The black region represents the W_LW_L strongly interacting physics.

2) Representative diagrams for backgrounds to the W_LW_L signal: (a) EW processes; (b) lowest-order QCD processes, with possible additional QCD-jet radiation; and (c) top quark backgrounds.

3) Invariant mass distributions for the "gold-plated" leptonic final states that arise from the processes $pp \to ZZX$, $pp \to W^+W^-X$, $pp \to W^+ZX$ and $pp \to W^+W^+X$, for $\sqrt{s} = 40$ TeV and an annual SSC luminosity of 10 fb^{-1}. The longitudinally-polarized signal is plotted above the summed background. The mass variable of x-axis is in units of GeV, and the bin size is 50 GeV.
   a) SM with a 1 TeV Higgs boson;
   b) $O(4)$ model with $\Lambda = 3$ TeV;
   c) Chirally coupled scalar with $M_S = 1$ TeV, $\Gamma_S = 350$ GeV;
   d) Chirally coupled vector with $M_V = 2$ TeV, $\Gamma_V = 700$ GeV;
   e) Chirally coupled vector with $M_V = 2.5$ TeV, $\Gamma_V = 1300$ GeV;
   f) Nonresonant model unitarized following Chanowitz and Gaillard;
   g) Nonresonant model unitarized by the K-matrix prescription;
   h) $\mathcal{O}(p^4)$ nonresonant model with delayed unitarity violation, unitarized by the K-matrix prescription.

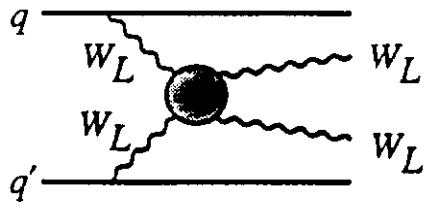

Fig. 1

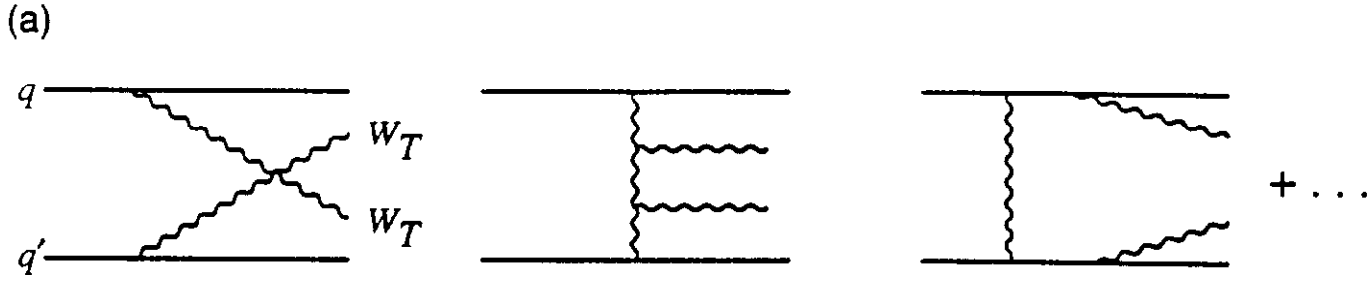

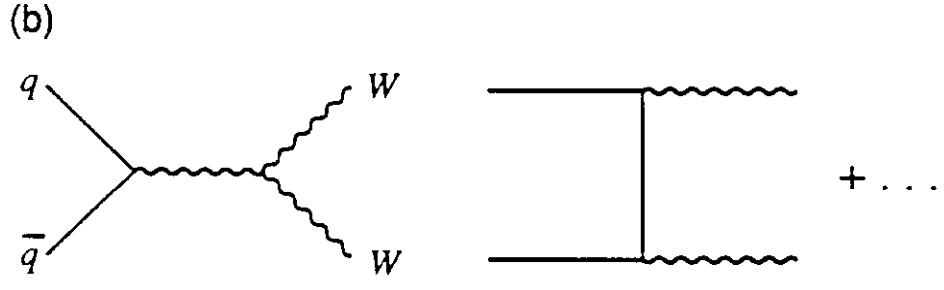

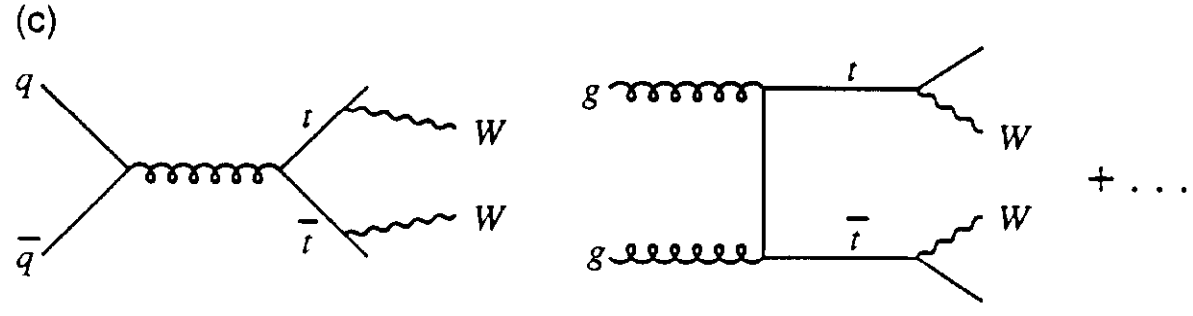

Fig. 2

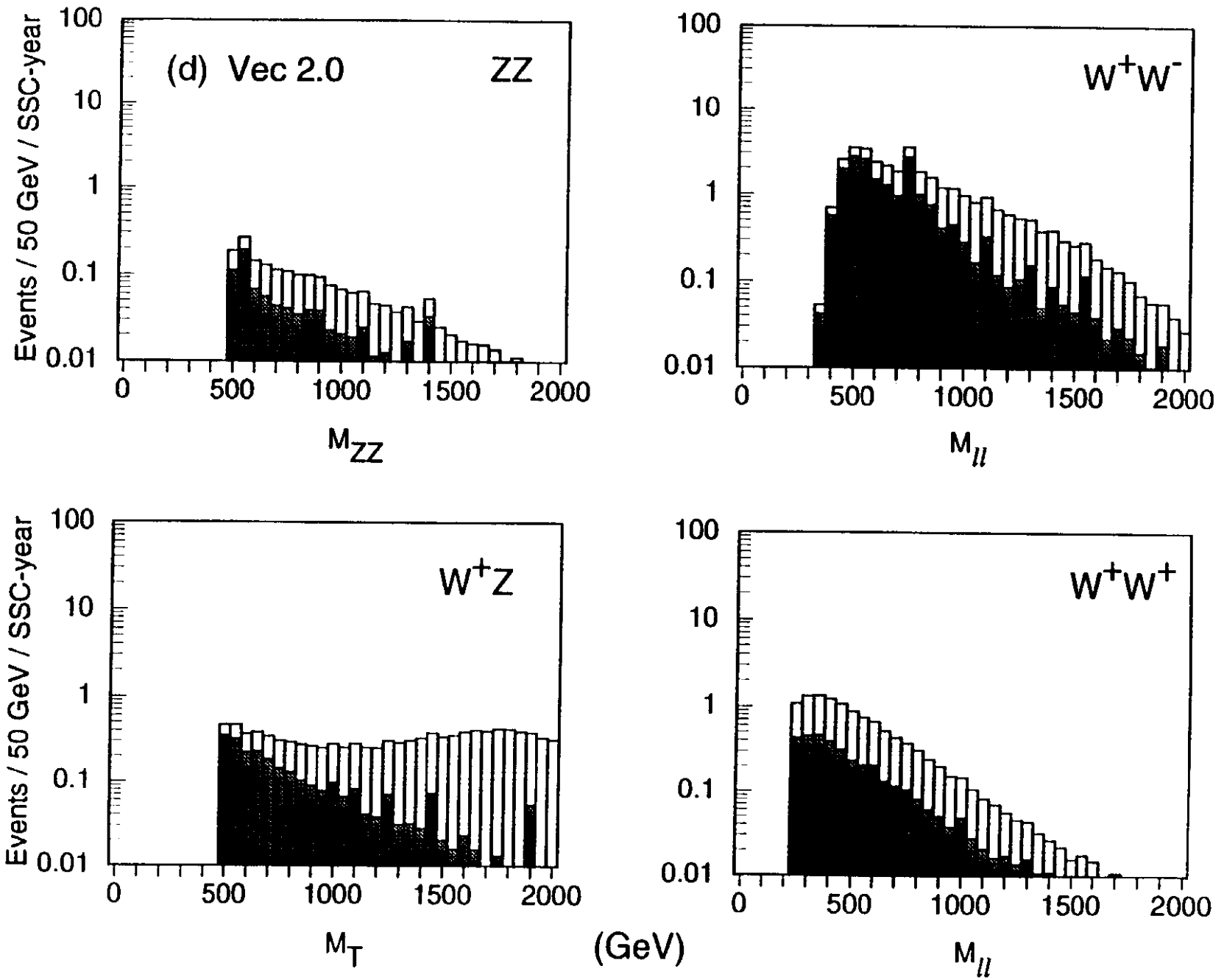
(d) Vec 2.0
ZZ
W+W-
W+Z
W+W+
Events / 50 GeV / SSC-year
100
10
1
0.1
0.01
0
500
1000
1500
2000
MZZ
Mll
MT
(GeV)

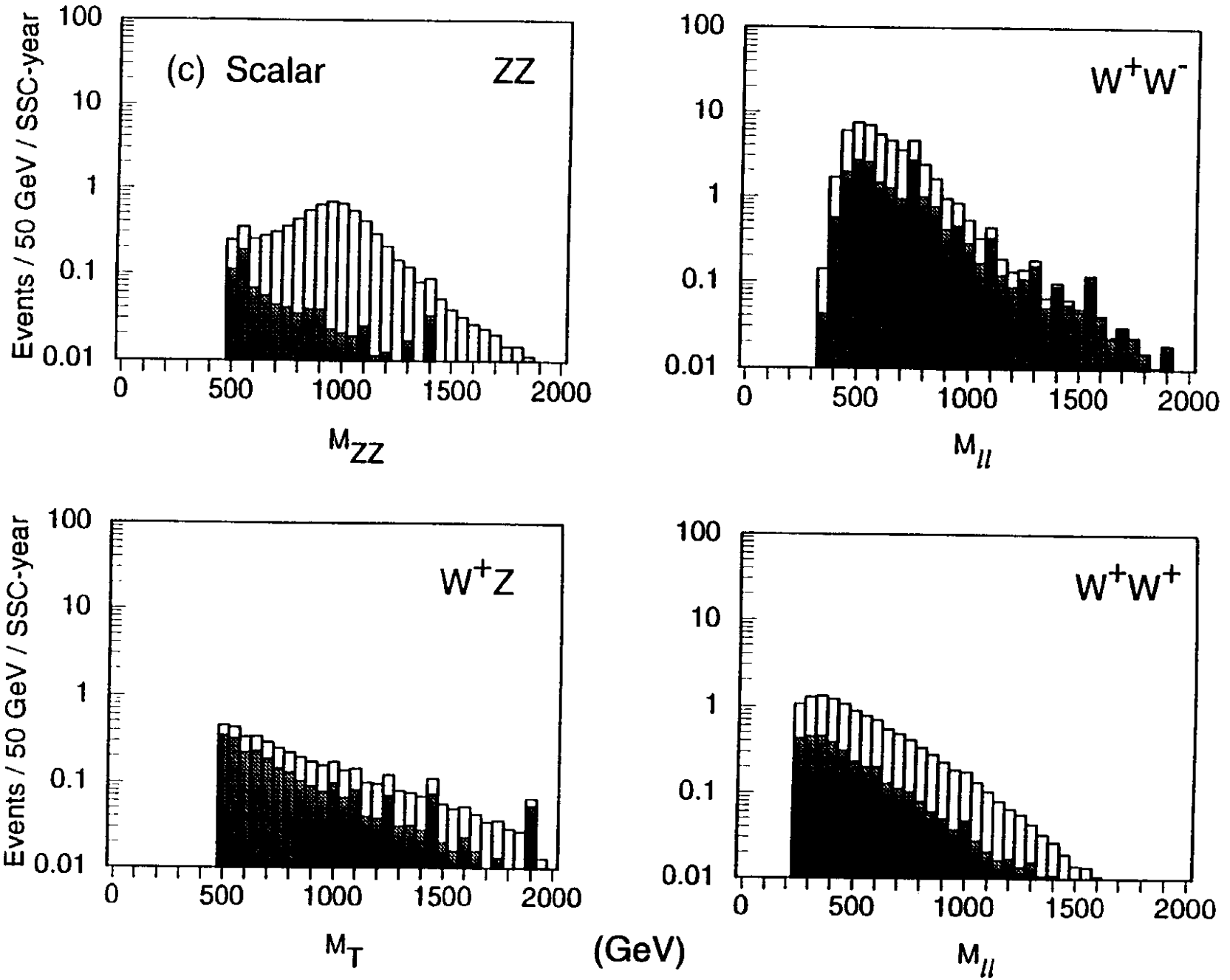
(c) Scalar
ZZ
W+W-
W+Z
W+W+
Events / 50 GeV / SSC-year
100
10
1
0.1
0.01
0
500
1000
1500
2000
MZZ
Mll
MT
(GeV)

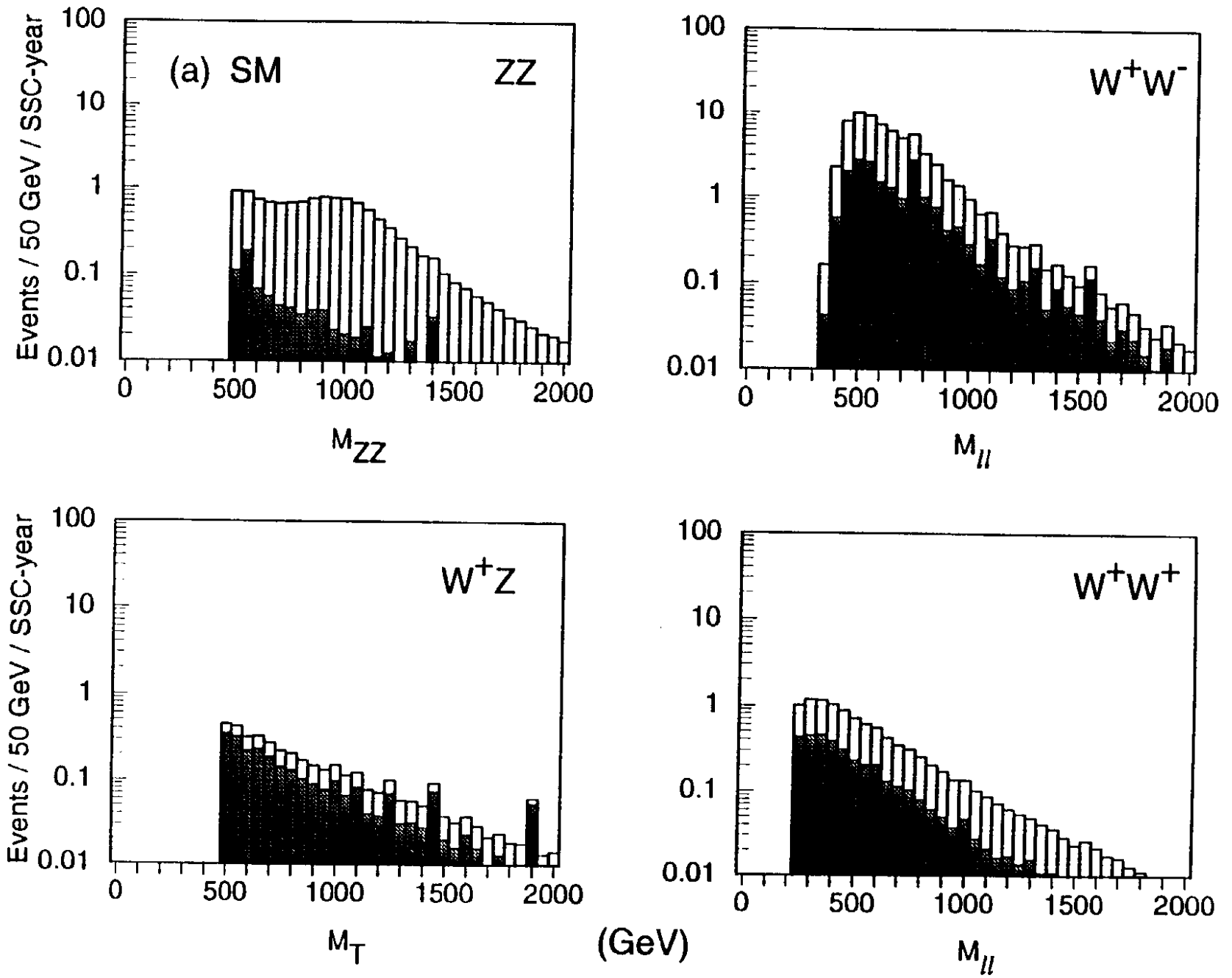
(a) SM
ZZ
W^+W^-
W^+Z
W^+W^+
Events / 50 GeV / SSC-year
100
10
1
0.1
0.01
0
500
1000
1500
2000
M_{ZZ}
M_{ll}
M_T
(GeV)

Fig. 3

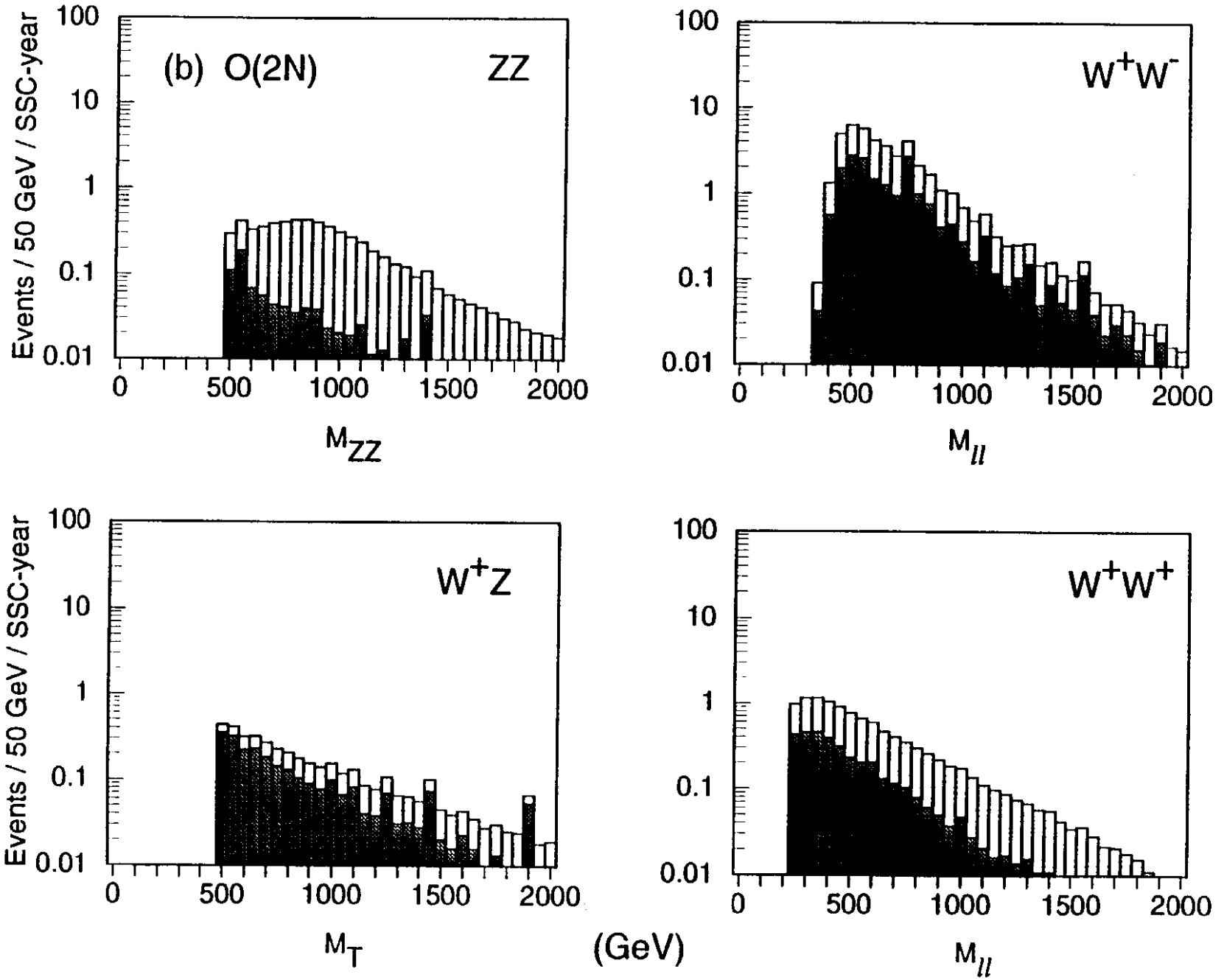
(b) O(2N)
ZZ
W+W-
W+Z
W+W+
Events / 50 GeV / SSC-year
100
10
1
0.1
0.01
0
500
1000
1500
2000
MZZ
Mll
MT
(GeV)

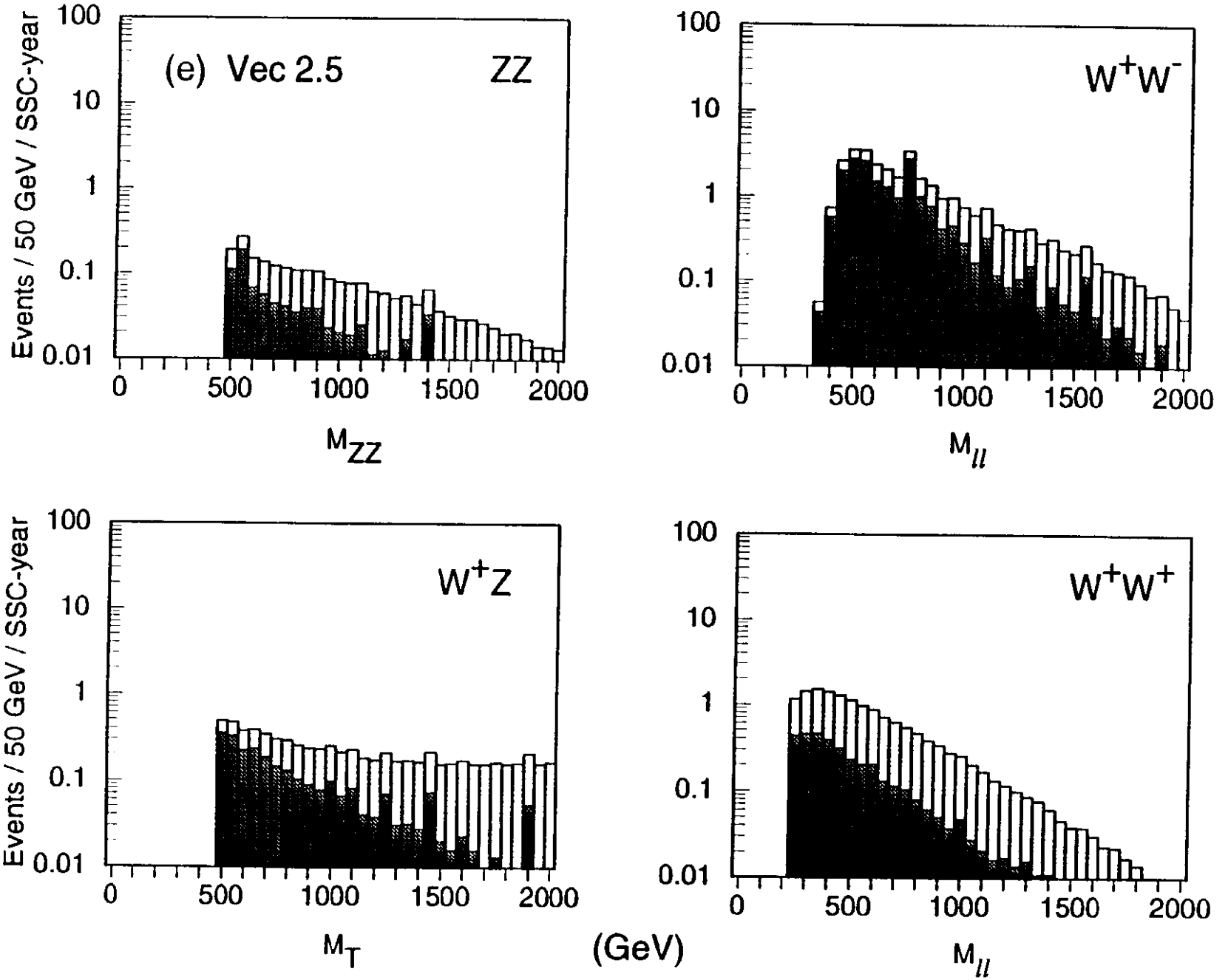
(e) Vec 2.5
ZZ
W^+W^-
W^+Z
W^+W^+
Events / 50 GeV / SSC-year
100
10
1
0.1
0.01
0
500
1000
1500
2000
M_{ZZ}
M_{ll}
M_T
(GeV)

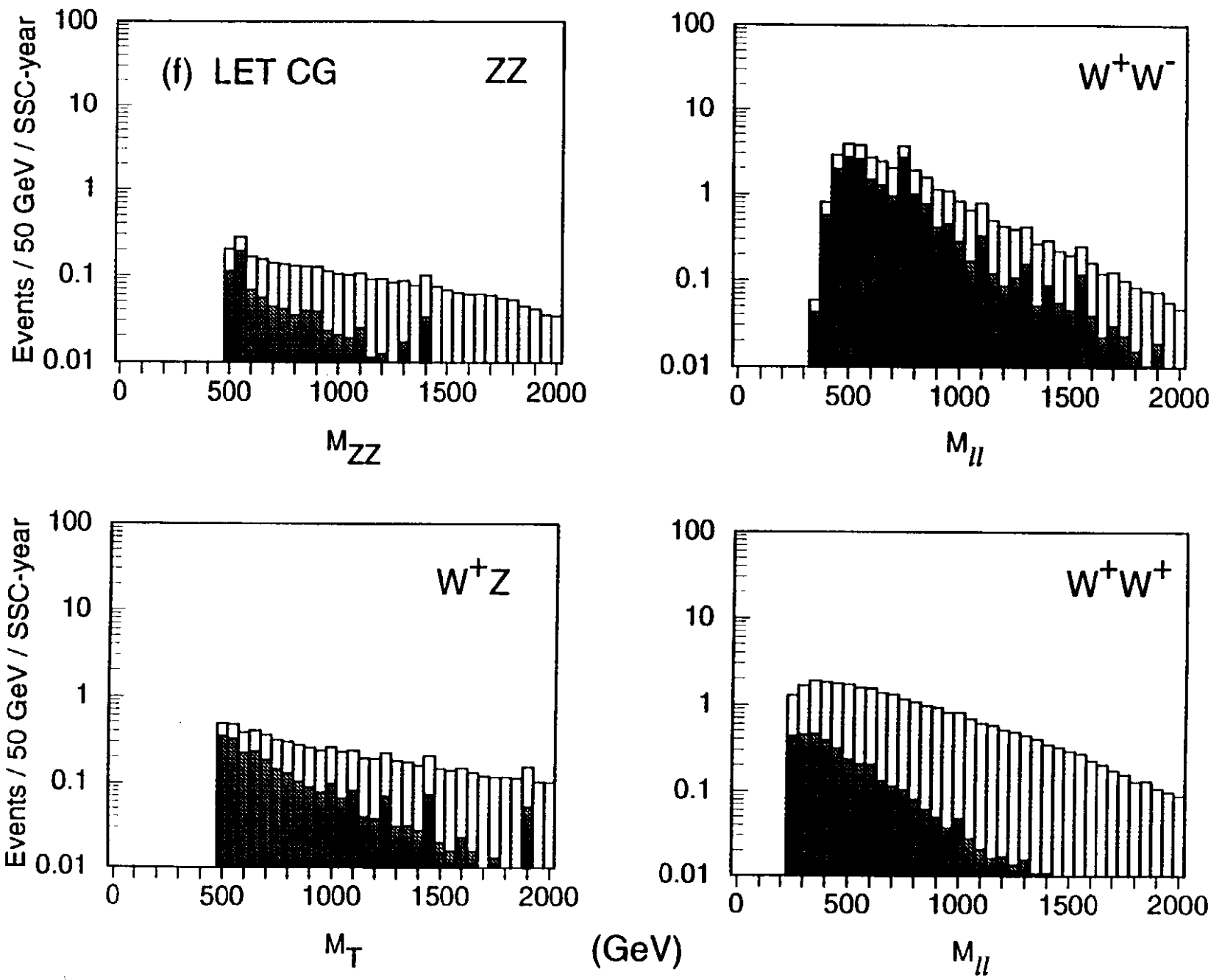
(f) LET CG
ZZ
W+W-
W+Z
W+W+
Events / 50 GeV / SSC-year
100
10
1
0.1
0.01
0
500
1000
1500
2000
MZZ
Mll
MT
(GeV)

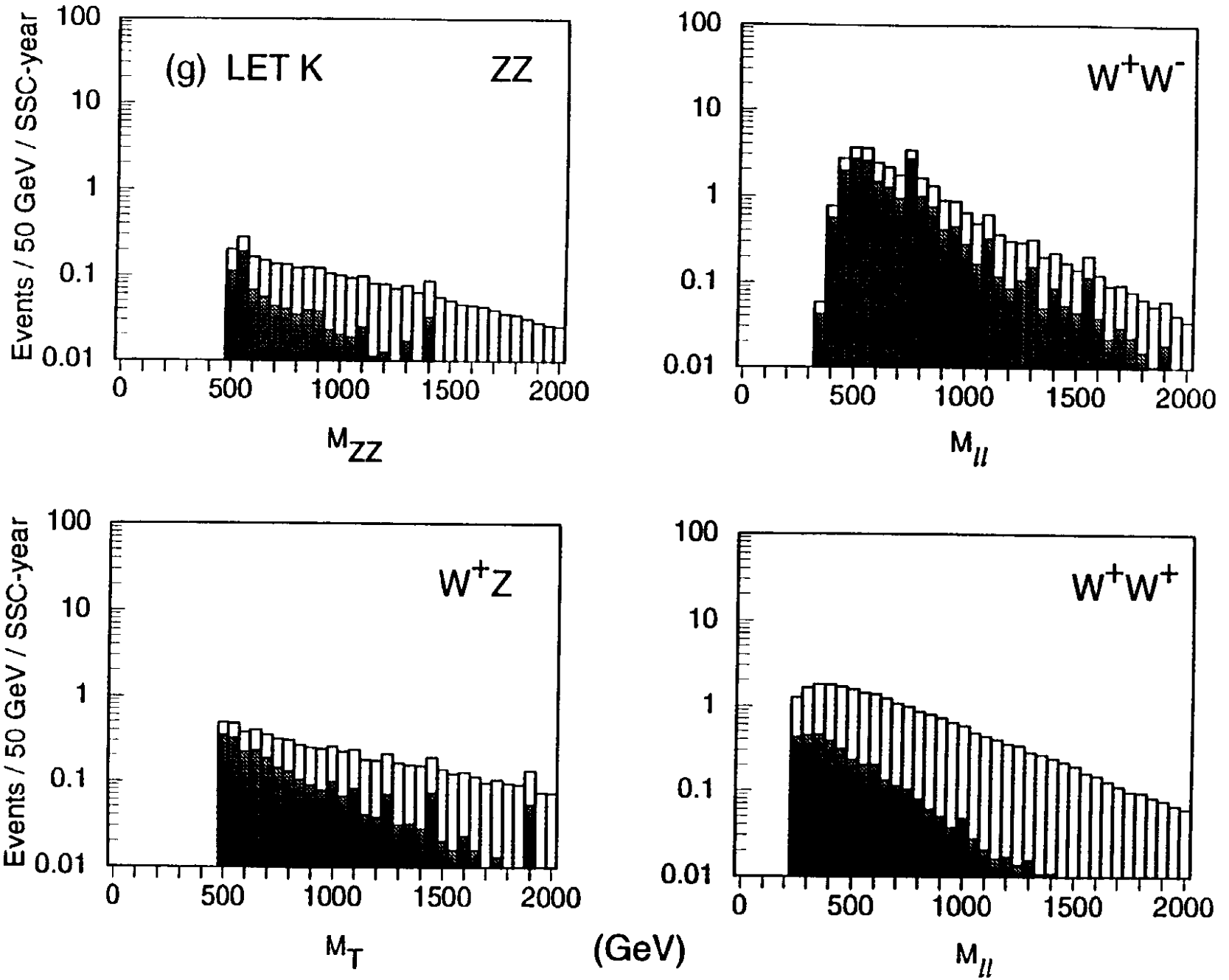
(g) LET K
ZZ
W+W-
W+Z
W+W+
Events / 50 GeV / SSC-year
100
10
1
0.1
0.01
0
500
1000
1500
2000
MZZ
Mll
MT
(GeV)

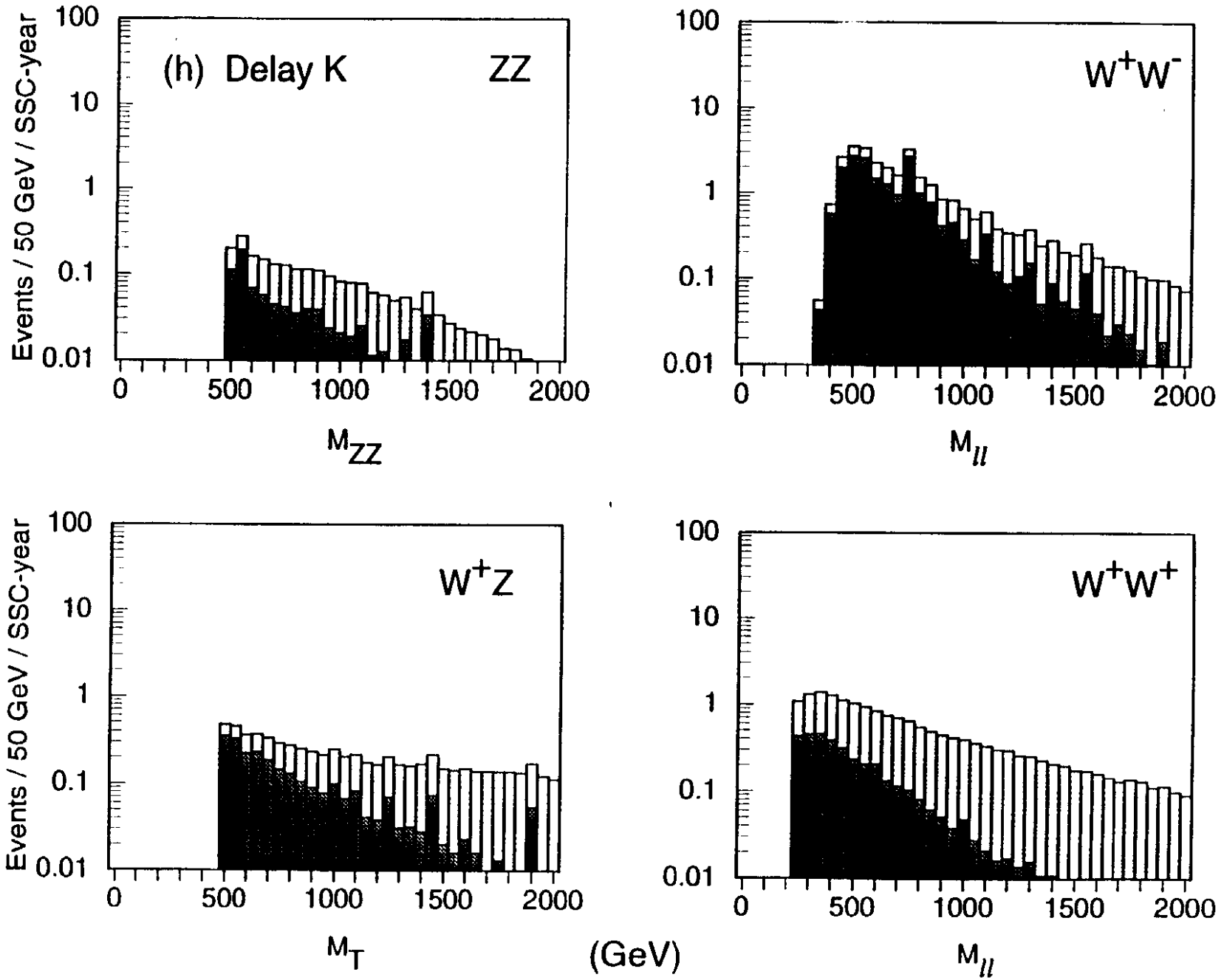
(h) Delay K
ZZ
W^+W^-
W^+Z
W^+W^+
Events / 50 GeV / SSC-year
100
10
1
0.1
0.01
0
500
1000
1500
2000
M_{ZZ}
M_{ll}
M_T
(GeV)

MEDICAL PLAN ENROLLMENT HISTORY

	1993		1994		1995		1996		1997	
Active										
PPO	1129	48.0%	1093	47.8%	1052	47.8%	1016	47.3%	977	47.3%
POS	125	5.3%	123	5.4%	115	5.2%	119	5.5%	126	6.1%
HMO IL*	1013	43.1%	991	43.3%	965	43.8%	951	44.2%	901	43.6%
Rush	84	3.6%	80	3.5%	71	3.2%	64	3.0%	62	3.0%
Total	2351		2287		2203		2150		2066	
PPO		48.0%		47.8%		47.8%		47.3%		47.3%
HMO		52.0%		52.2%		52.2%		52.7%		52.7%

* Before merger in 1996: HMO IL 425 & Dreyer 588 in 1993
HMO IL 427 & Dreyer 564 in 1994
HMO IL 410 & Dreyer 555 in 1995

	1993		1994		1995		1996		1997	
Retiree										
PPO	309	94.5%	327	90.3%	353	90.3%	372	89.6%	400	88.7%
POS	0	0.0%	0	0.0%	0	0.0%	0	0.0%	1	0.2%
HMO IL*	16	4.9%	33	9.1%	36	9.2%	40	9.6%	48	10.6%
Rush	2	0.6%	2	0.6%	2	0.5%	3	0.7%	2	0.4%
Total	327		362		391		415		451	
PPO		94.5%		90.3%		90.3%		89.6%		88.7%
HMO		5.5%		9.7%		9.7%		10.4%		11.3%

* Before merger in 1996: HMO IL 6 & Dreyer 10 in 1993
HMO IL 9 & Dreyer 24 in 1994
HMO IL 12 & Dreyer 24 in 1995

DENTAL ENROLLMENT HISTORY

	1993		1994		1995		1996		1997	
Traditional	1808	76.4%	1761	76.5%	1659	75.5%	1581	73.9%	1489	73.0%
DMO	557	23.6%	540	23.5%	537	24.5%	557	26.1%	551	27.0%
Total	2365		2301		2196		2138		2040	